NACA RM L56B02

62

NACA

RESEARCH MEMORANDUM

TRANSONIC INVESTIGATION OF THE EFFECTIVENESS AND LOADING CHARACTERISTICS OF A FLAP-TYPE AILERON WITH AND WITHOUT PADDLE BALANCES ON AN UNSWEPT-WING—FUSELAGE MODEL

By Gerald Hieser

Langley Aeronautical Laboratory
Langley Field, Va.

NATIONAL ADVISORY COMMITTEE
FOR AERONAUTICS

WASHINGTON

April 13, 1956

NACA RM L56B02

NATIONAL ADVISORY COMMITTEE FOR AERONAUTICS

RESEARCH MEMORANDUM

TRANSONIC INVESTIGATION OF THE EFFECTIVENESS AND LOADING CHARACTERISTICS OF A FLAP-TYPE AILERON WITH AND WITHOUT PADDLE BALANCES ON AN UNSWEPT-WING—FUSELAGE MODEL

By Gerald Hieser

SUMMARY

An investigation has been conducted at the Langley 16-foot transonic tunnel for the purpose of investigating the effectiveness and loading characteristics of an aileron mounted on an unswept-wing—body configuration. The flap-type outboard aileron was tested with and without paddle balances at Mach numbers from 0.70 to 1.05 and angles of attack from 0° to 14°. The test Reynolds number, based on wing mean aerodynamic chord, varied from about 5.5×10^6 to 6.5×10^6.

Results of the investigation indicate that with increasing Mach number at an angle of attack of 0°, the aileron effectiveness is nearly constant until a Mach number of 0.94 is reached, after which a rapid decrease in effectiveness occurs. At Mach numbers from 0.98 to 1.05, the paddle balances reduce the aileron hinge-moment coefficient by about 22 percent at an angle of attack of 0°. The largest increase in drag coefficient due to addition of paddle balances to one aileron amounts to about 0.002.

INTRODUCTION

Because theory for predicting effectiveness and loading characteristics of lateral controls is inadequate at transonic speeds, recourse must be made to experimental research to supply such information. Accordingly, some lateral control investigations at transonic speeds have been conducted by the NACA on small-scale models by utilizing the transonic bump and wing flow techniques (see, for example, refs. 1 to 3).

A program is now in progress at the Langley 16-foot transonic tunnel for the purpose of obtaining the effectiveness and loading of controls

C[redacted]I,

on relatively large scale unswept, sweptback, and delta wings at Mach numbers up to and slightly above 1.0. The present report includes the results from tests of a 25-percent-chord, 40-percent-semispan outboard aileron mounted on an unswept-wing model employing a wing with an aspect ratio of 4.0, a taper ratio of 0.5, and NACA 65A004 airfoil sections. Effectiveness and loading characteristics were obtained with and without delta-shaped paddle balances mounted above and below the aileron. The tests covered Mach numbers from 0.70 to 1.05 and angles of attack from 0° to 14°. The test Reynolds number based on wing mean aerodynamic chord varied from about 5.5×10^6 to 6.5×10^6.

SYMBOLS

The model forces and moments have been reduced to the stability system of axes. Model lateral coefficients and the aileron data obtained with the model inverted have been converted to the equivalent of an upright model with the control on the right wing. Positive hinge moment is defined as a nose-up moment for the aileron on the right wing.

b wing span

b_a span of aileron

c local wing chord

c' wing mean aerodynamic chord, $\frac{2}{S}\int_0^{b/2} c^2 dy$

$\bar{c}_a$ average chord of aileron

C_D drag coefficient, $\frac{\text{Drag}}{qS}$

C_h aileron hinge-moment coefficient, $\frac{\text{Hinge moment about hinge line}}{2qM'}$

C_L lift coefficient, $\frac{\text{Lift}}{qS}$

C_l rolling-moment coefficient, $\frac{\text{Rolling moment}}{qSb}$

[redacted]

C_m pitching-moment coefficient, $\frac{\text{Pitching moment about mean aerodynamic quarter-chord}}{qSc'}$

C_n yawing-moment coefficient, $\frac{\text{Yawing moment}}{qSb}$

C_{N_a} aileron normal-force coefficient, $\frac{\text{Aileron normal force}}{qS_a}$

C_Y lateral-force coefficient, $\frac{\text{Lateral force}}{qS}$

$$C_{h_\alpha} = \left(\frac{\partial C_h}{\partial \alpha}\right)_{\delta_a}$$

$$C_{h_{\delta_a}} = \left(\frac{\partial C_h}{\partial \delta_a}\right)_{\alpha}$$

$$C_{l_{\delta_a}} = \left(\frac{\partial C_l}{\partial \delta_a}\right)_{\alpha}$$

M free-stream Mach number

M' area moment of aileron rearward of and about aileron hinge axis

q free-stream dynamic pressure

S wing area

S_a area of aileron

x' distance from aileron hinge line to aileron center of pressure measured in the aileron chord plane and parallel to the model plane of symmetry (positive to rear of hinge line)

y lateral distance measured perpendicular to plane of symmetry

y' lateral distance to aileron center of pressure measured from inboard edge of aileron (positive outboard)

α angle of attack of model (fuselage center line)

δ_a aileron deflection angle relative to wing chord plane, measured parallel to the plane of symmetry (positive when trailing edge is down)

δ_b paddle balance deflection angle relative to aileron chord plane (positive when trailing edge is down). (Upper and lower balances remain parallel at all deflections.)

Λ sweep angle, deg

The subscripts δ_a and α outside the parentheses denote the parameters maintained constant. The subscript L.E. denotes wing leading edge.

MODEL AND APPARATUS

Model

Geometric details and pertinent dimensions of the basic wing-fuselage combination are given in figure 1. A table of the fuselage ordinates is given in reference 4. Photographs of the sting-supported model installed in the tunnel and views of the aileron and paddle balances are shown as figure 2. The steel wing, which has zero sweep of the 0.50-chord line, was mounted in a midwing position and has no geometric twist, incidence, or dihedral.

Details and dimensions of the aileron and paddle balances are shown in figure 3. The unsealed trailing-edge aileron is hinged at the 0.75-wing-chord line and has 0.045-aileron-chord overhang. The inboard edge of the aileron is located at the 58-percent-wing-semispan station and the outboard edge at the 98-percent station. Three different ailerons were utilized to obtain deflected aileron configurations. These ailerons were geometrically similar except for the hinges which were strain-gage beams machined as part of the aileron. The beams were bent at different angles on the three ailerons to permit nominal (no load) deflections of 0°, -10°, and -15°. A positive deflection angle of 10° was obtained by inverting the entire model with the -10° aileron installed.

The strain-gage beams were shielded from the airstream by small brass cover plates mounted on the ailerons above and below the hinge beams. The plates extended from the hinge line rearward a distance of about $\frac{3}{4}$ inch and were $1\frac{3}{4}$ inches wide. They were contoured so that the

maximum height above the wing contour occurred just behind the hinge line and was about $\frac{1}{16}$ inch. All plates were faired to a smooth contour as can be seen in the photograph of figure 2(c) and in the sketch of figure 3.

The paddle balances, mounted above and below the aileron (figs. 2 and 3), were located ahead of the hinge line at the 0.378-span station of the aileron. The angle of the paddles δ_b was 0° on the 0° aileron. Two additional sets of paddles were utilized for tests with the 10° aileron, one set mounted at an angle of $\delta_b = 5^\circ$ and the other at $\delta_b = 10^\circ$ on the aileron.

Instrumentation

The overall model forces and moments were measured by a six-component internal strain-gage balance. Aileron normal forces and hinge moments were measured by strain-gage balances mounted on the hinge beams. Angle of attack was obtained from a strain-gage attitude transmitter mounted in the nose of the model. Pressures at the model base were measured by two orifices mounted flush with the internal surface of the fuselage about 2 inches ahead of the fuselage base.

Tunnel and Model Support

The tests were conducted in the Langley 16-foot transonic tunnel, which has an octagonal slotted test section permitting a continuous variation in speed to Mach numbers slightly above 1.0.

The sting support system, which is described in reference 5, is arranged so that the model is located near the center of the tunnel at all angles of attack.

TESTS

Simultaneous measurements of model forces and moments, and aileron hinge moment and normal force were obtained during tests of the model without paddle balances at the angles and Mach numbers given in the following table:

Mach number, M	Angle of attack, α, at -			
	Nominal δ_a = -15	Nominal δ_a = -10	Nominal δ_a = 0	Nominal δ_a = 10 (model inverted)
0.70	----------	0 to 14.0	0 to 14.0	0 to 14.0
.80	----------	0 to 13.8	0 to 14.0	0 to 14.0
.90	-0.1 to 11.5	0 to 11.4	0 to 11.5	0 to 11.6
.92	-.1 to 11.6	0 to 11.4	0 to 11.6	0 to 11.6
.94	-.1 to 13.8	0 to 13.8	0 to 11.6	0 to 8.0
.96	0 to 13.7	0 to 13.8	0 to 11.7	0 to 8.0
.98	-.1 to 11.6	-0.1 to 11.7	0 to 11.7	0 to 8.0
1.00	-.1 to 13.8	0 to 13.7	0 to 11.7	0 to 8.0
1.05	-.1 to 8.0	0 to 7.9	0 to 8.0	0 to 6.0

Model and aileron forces and moments were obtained with the paddle balances installed for the following angles and Mach numbers:

Mach number, M	Angle of attack, α, at -		
	Nominal δ_a = 0	Nominal δ_a = 10	
	δ_b = 0	δ_b = 5	δ_b = 10
0.70	----------	0, 4.0, 8.0, 10.0, 12.0, 14.0	0, 4.0, 8.0, 10.0, 12.0, 14.0
.80	----------	0, 4.0, 8.0, 10.0, 12.0, 14.0	0, 4.0, 8.0, 10.0, 12.0, 14.0
.94	----------	0, 4.0, 8.0, 11.7	0, 4.1
.98	0, 4.0, 8.0	0, 4.0, 8.0	0, 4.1, 8.1
1.00	0, 4.0, 8.0	0, 4.0, 8.0	0, 4.0, 8.0
1.05	0, 4.0, 8.0	0, 4.0, 8.0	

The test Reynolds number based on wing mean aerodynamic chord varied from about 5.5×10^6 to about 6.5×10^6 (see fig. 4).

ACCURACY

The measurement of Mach number in the test region is believed to be accurate within ±0.002 (ref. 6), and the angles of attack presented are believed to be correct within ±0.1°.

The aileron deflection angles were determined from the nominal angle and an additional angle due to deflection under loading conditions. This additional angle was determined from a static loading calibration. The resulting aileron deflection angles δ_a are believed to be correct within ±0.2°.

Lift and drag data have been adjusted to the condition of free-stream static pressure at the model base. Base pressure coefficients for the model without an aileron or paddle balances are given in reference 4. Deflecting the aileron and adding paddle balances had a relatively small effect on the base pressures, and therefore, the coefficients are not presented in this report.

No adjustments for sting interference or aeroelasticity have been applied to the model aerodynamics forces and moments or to the aileron force and moment measurements. The maximum twist of the wing with no aileron deflection within the range of test conditions reported has been estimated as 0.6° (see ref. 4). Tunnel boundary-induced effects for wing-body combinations are believed to be negligible in this slotted test section (ref. 7).

The accuracy of the measured coefficients based on balance accuracy and repeatability of data is believed to be within the following limits:

C_L	±0.01
C_D at low lift coefficients	±0.001
C_D at high lift coefficients	±0.003
C_m	±0.003
C_l	±0.001
C_n	±0.0005
C_Y	±0.001
C_h	±0.02
C_{N_a}	±0.04

RESULTS AND DISCUSSION

Model force and moment characteristics and the aileron hinge-moment and normal-force coefficients are presented in figures 5 to 12. The chordwise and spanwise centers of load on the aileron are given in figures 13 and 14, respectively. Figures 15 to 24 present the analysis prepared from the basic data.

Effectiveness and Loading of Aileron Without Paddle Balances

Effectiveness.- The variation of rolling-moment coefficient with aileron deflection at various angles of attack and Mach numbers is shown in figure 8. As indicated by the data at the deflections of these tests, the curves are linear, or nearly linear, at all angles of attack investigated and Mach numbers up to 1.05, the limit of the tests. Although no data were obtained at small deflection angles, it is believed that no discontinuities in the rolling-moment curves exist for a flap-type aileron on a thin unswept wing near zero aileron deflection. Generally, the deviations from straight lines in the direction of a lower aileron effectiveness are not very large and occur at deflections greater than about 10° at Mach numbers up to about 0.94. At higher Mach numbers essentially no loss in effectiveness occurs with increasing deflection up to the largest deflections of the tests.

As shown in figure 15, the aileron effectiveness parameter $C_{l_{\delta_a}}$ at an angle of attack of zero remains nearly constant and has a value of about -0.0020 at Mach numbers from 0.70 to about 0.92. As the Mach number is increased to 0.94 a small increase in effectiveness occurs. Examination of wing pressure distributions in reference 4 for the present model with undeflected aileron reveals that the main wing shock is located at about the 0.75-chord station (hinge-line location) at a Mach number of 0.94 and an angle of attack of zero. As δ_a is increased from zero the shock probably moves back on the upper surface (positive deflections) or rearward on the lower surface (negative deflections), thereby increasing the load on the aileron and wing at a greater rate than at lower Mach numbers where the shock is ahead of the aileron. As the Mach number is increased above 0.94 the shock moves back to the trailing edge and changes in δ_a probably no longer affect the shock position. Furthermore, with completely supersonic flow over the aileron, changes in δ_a probably have little or no effect on the pressures ahead of the aileron; hence, the decrease in effectiveness.

The curves of figure 15 also indicate that the aileron effectiveness begins to decrease at progressively lower Mach numbers as the angle of

attack is increased. This decrease is a result of the rearward movement of the main wing shock with increasing angle of attack, which is characteristic of thin, unswept wings (ref. 4).

Loading.- The aileron hinge-moment and normal-force data of figures 11 and 12 show that despite the existence of both subsonic and supersonic flow and the associated shock formations and movements on the model at transonic speeds, the aileron loading variations with deflection are relatively uniform. In fact, the curves at low angles of attack are linear, or nearly linear, at all Mach numbers up to 1.05. Departures from linearity generally occur at the same conditions and are similar in character for both the hinge-moment and normal-force curves.

The aileron chordwise position of center of loading calculated from the normal-force and hinge-moment data is shown in figure 13. At angles of attack of 0° and 4° the center of load variation with deflection is small, as might be expected in view of the similarity between the hinge-moment and normal-force curves. This small variation is, of course, confined to regions where C_h and C_{N_a} are not near zero. As Mach number is increased the center of load generally moves rearward until a Mach number of about 0.98 is reached, after which its position is nearly constant. This rearward travel results from the rearward movement of the wing shock and the resultant transformation of the aileron load from a triangular shape to rectangular (ref. 8).

The effect of angle of attack, aileron deflection, and Mach number on the aileron spanwise center of load is presented in figure 14. Although the curves are somewhat erratic, several trends can be noted. Increasing angle of attack generally causes an inboard movement of load at $\delta_a = 0^\circ$, while an outboard movement results at negative deflections. For a positive aileron deflection or for the undeflected aileron increasing Mach number has little effect on the lateral center of load until a Mach number of 0.94 is reached where a rather abrupt inboard movement occurs. This inward shift averages about 5 percent of the aileron span. The effect of Mach number on the center of load at negative deflections is very small and no trend can be noted.

In order to show the effect of angle of attack on hinge-moment coefficient the data of figure 11 have been cross plotted and are presented in figures 16 and 17. At $M = 0.70$ and $\delta = 0^\circ$, the increase in C_h with angle of attack is gradual throughout the angle-of-attack range investigated (fig. 16). As shown by the pressure distributions of reference 4, the loading over the aileron remains triangular in shape and increases gradually with angle of attack. At $M = 0.80$ also the hinge moment increases gradually until an angle of about 9° is reached where C_h begins

[redacted]

to increase at a greater rate. The pressure distributions indicate that flow separation from the wing leading edge at about this angle results in an increase in the load over the trailing portion of the wing.

When the Mach number is increased from 0.90 to 0.96, C_h remains nearly zero at low angles of attack but increases rather abruptly at moderate angles. Note that the angle at which this increase begins is progressively lower as the Mach number is increased. At each Mach number the main wing shock is located near the aileron leading edge at the angle of attack where the hinge-moment coefficient begins to increase rapidly. The increase in loading with α is caused by the rearward movement of the shock, which not only increases the trailing-edge load, but also causes a change in the loading shape from triangular to trapezoidal or rectangular. At Mach numbers above 0.96 the shock is at the trailing edge at all angles of attack and there is a less abrupt change in the slope of the C_h against α curve.

Aileron deflection has little effect on the variation of hinge-moment coefficient with angle of attack (fig. 17). At a deflection of -12°, however, the increase in C_h with δ_a is generally somewhat more gradual than at lower deflections.

The values of the hinge-moment parameter $C_{h_{\delta_a}}$ presented in figure 18 were obtained from the curves of figure 11 as average slopes at $\delta_a = 0^\circ$. At an angle of attack of 0°, $C_{h_{\delta_a}}$ increases from about -0.011 at $M = 0.70$ to about -0.037 at $M = 0.96$ after which a slight decrease occurs. Increasing the angle of attack to 4° has little effect on the trend of the curve. At an angle of attack of 8°, however, the Mach number at which a rapid increase in $C_{h_{\delta_a}}$ occurs is reduced from about 0.92 to about 0.85. Angle of attack has very little effect on the values of this parameter at the low and high ranges of Mach number. The gradual increase in $C_{h_{\delta_a}}$ at Mach numbers from 0.70 to about 0.92 at $\alpha = 0^\circ$ and 4°, and at Mach numbers from 0.70 to 0.85 for the $\alpha = 8^\circ$ curve is due to compressibility. As Mach number is increased, however, the rapid increase in $C_{h_{\delta_a}}$ probably results from an increased rate of rearward movement of the wing shock over the aileron as the aileron is deflected. After a Mach number of about 0.96 is reached the flow over the aileron is completely supersonic at all deflections and only small changes in $C_{h_{\delta_a}}$ occur as M is increased.

The parameter C_{h_α} presented in figure 18 was obtained from the linear portion of the curves in figure 16 at low angles of attack. This

parameter is very small at Mach numbers up to about 0.96. The wing shock remains ahead of the aileron at small angles of attack and, therefore, the load at the trailing portion of the wing does not increase until higher angles are attained. At Mach numbers from 0.96 to 1.05, C_{h_α} increases rapidly reaching a value of about -0.012. At these Mach numbers the flow over the aileron is completely supersonic and the load increases with increasing angle of attack.

Effect of Paddle Balances

The delta-shaped paddle balances were designed to balance about 25 percent of the aileron hinge moment. In order to utilize relatively small paddles, geared-type balances were simulated by mounting them at an angle 50 percent greater than the aileron deflection angle with respect to the wing chord plane, that is, $\frac{d(\delta_a + \delta_b)}{d\delta_a} = \frac{\delta_a + \delta_b}{\delta_a} = 1.5$. It should be noted, however, that the gear ratio is not quite constant in this case, because the aileron deflection δ_a varies somewhat with loading while δ_b remains very nearly constant.

In order to obtain further information on the effectiveness of the paddles, one test was made at an aileron deflection of 10° with the paddles mounted at +10° with respect to the aileron, resulting in a balance-to-aileron gear ratio of 2 to 1. The following discussion, however, refers to data obtained with the balances geared at 1.5 to 1 unless otherwise noted.

Aerodynamic characteristics.- Drag measurements of the model with the paddle balances installed were obtained at Mach numbers of 0.98, 1.00, and 1.05 only. As shown in figure 19 the largest increase in drag coefficient due to the paddle balances (gear ratio = 1.5) is about 0.002. This increment is, of course, only half the amount that would occur for the configuration with paddle balances on both ailerons.

Addition of the paddle balances to the model results in only minor changes in rolling-moment coefficient or aileron effectiveness at Mach numbers from 0.98 to 1.05 (fig. 20). The effect on rolling-moment coefficient of increasing the paddle angle from 5° with respect to the aileron (geared 1.5 to 1) to 10° (geared 2 to 1) at a nominal δ_a of 10° is shown in figure 21. The rolling moment is increased by increasing the paddle-balance angle at a Mach number of 0.70 and to a lesser extent at a Mach number of 0.80. However, as the Mach number is increased to 0.94 and 1.00, the paddle-balance angle has little effect on rolling moment.

Aileron loading.- The aileron normal-force coefficient at Mach numbers of 0.98, 1.00, and 1.05 (fig. 22) is affected very little by the paddle balances. Apparently the paddles bend the streamlines such that the load on the aileron is reduced an amount almost equal to the normal load on the paddles.

The data of figure 23 indicate that the paddle balances reduce the hinge moment by about 22 percent at an angle of attack of zero and, as shown in figure 18, reduce $C_{h_{\delta_a}}$ at all angles of attack by about the same percentage. As stated previously, the balances were designed to decrease the aileron hinge moments by about 25 percent. The calculations of paddle-balance effectiveness are, therefore, in relatively good agreement with the measured values. These calculations were performed by utilizing supersonic lift and drag data of a delta-wing plan form and the appropriate moment arms.

The variation of aileron hinge-moment coefficient with paddle-balance angle at a nominal aileron deflection of 10° is shown in figure 24. Although the quantitative effect of δ_b on hinge moment is somewhat erratic, increasing the paddle-balance angle from 5° to 10° reduces C_h at all Mach numbers and angles of attack shown.

CONCLUSIONS

Results of a transonic investigation of the effectiveness and loading characteristics of a flap-type aileron on an unswept-wing—fuselage model with and without paddle balances installed lead to the following conclusions:

1. With increasing M at $\alpha = 0^\circ$ the aileron effectiveness $C_{l_{\delta_a}}$ is nearly constant at a value of about -0.0020 until a Mach number of 0.94 is reached after which a decrease occurs. Increasing the angle of attack reduces the Mach number at which a decrease in effectiveness begins.

2. The hinge-moment parameter $C_{h_{\delta_a}}$ at $\alpha = 0^\circ$ varies from about -0.011 at $M = 0.70$ to about -0.037 at $M = 0.96$ after which a slight decrease occurs. Increasing the angle of attack to 8° has little effect on the general trend of the curve.

3. The parameter C_{h_α} is very small at Mach numbers up to about 0.96 after which a rapid increase occurs reaching a value of about -0.012 at $M = 1.05$.

[redacted]

4. At Mach numbers from 0.98 to 1.05 the paddle balances reduce the hinge-moment parameter $C_{h_{\delta_a}}$ by about 22 percent and reduce the hinge-moment coefficient at $\alpha = 0^\circ$ by about the same percentage.

5. The greatest increase in drag coefficient due to the addition of paddle balances to one aileron amounts to about 0.002.

Langley Aeronautical Laboratory,
National Advisory Committee for Aeronautics,
Langley Field, Va., January 24, 1956.

[redacted]

1. Hammond, Alexander D.: Lateral Control Investigation of Flap-Type Controls on a Wing With Unswept Quarter-Chord Line, Aspect Ratio 4, Taper Ratio 0.6, and NACA 65A006 Airfoil Section. Transonic-Bump Method. NACA RM L50A03, 1950.

2. Turner, Thomas R., Lockwood, Vernard E., and Vogler, Raymond D.: Aerodynamic Characteristics at Subsonic and Transonic Speeds of a 42.7° Sweptback Wing Model Having an Aileron With Finite Trailing-Edge Thickness. NACA RM L8K02, 1949.

3. Johnson, Harold I.: Measurements of Aerodynamic Characteristics at Transonic Speeds of an Unswept and Untapered NACA 65-009 Airfoil Model of Aspect Ratio 3 With 1/4-Chord Plain Flap by the NACA Wing-Flow Method. NACA RM L53D21, 1953.

4. Hieser, Gerald, Henderson, James H., and Swihart, John M.: Transonic Aerodynamic and Loads Characteristics of a 4-Percent-Thick Unswept-Wing—Fuselage Combination. NACA RM L54B24, 1954.

5. Hallissy, Joseph M., and Bowman, Donald R.: Transonic Characteristics of a 45° Sweptback Wing-Fuselage Combination. Effect of Longitudinal Wing Position and Division of Wing and Fuselage Forces and Moments. NACA RM L52K04, 1953.

6. Ward, Vernon G., Whitcomb, Charles F., and Pearson, Merwin D.: Air-Flow and Power Characteristics of the Langley 16-Foot Transonic Tunnel With Slotted Test Section. NACA RM L52E01, 1952.

7. Whitcomb, Charles F., and Osborne, Robert S.: An Experimental Investigation of Boundary Interference on Force and Moment Characteristics of Lifting Models in the Langley 16- and 8-Foot Transonic Tunnels. NACA RM L52L29, 1953.

8. Runckel, Jack F., and Gray, W. H.: An Investigation of Loads on Ailerons at Transonic Speeds. NACA RM L55E13, 1955.

[redacted]

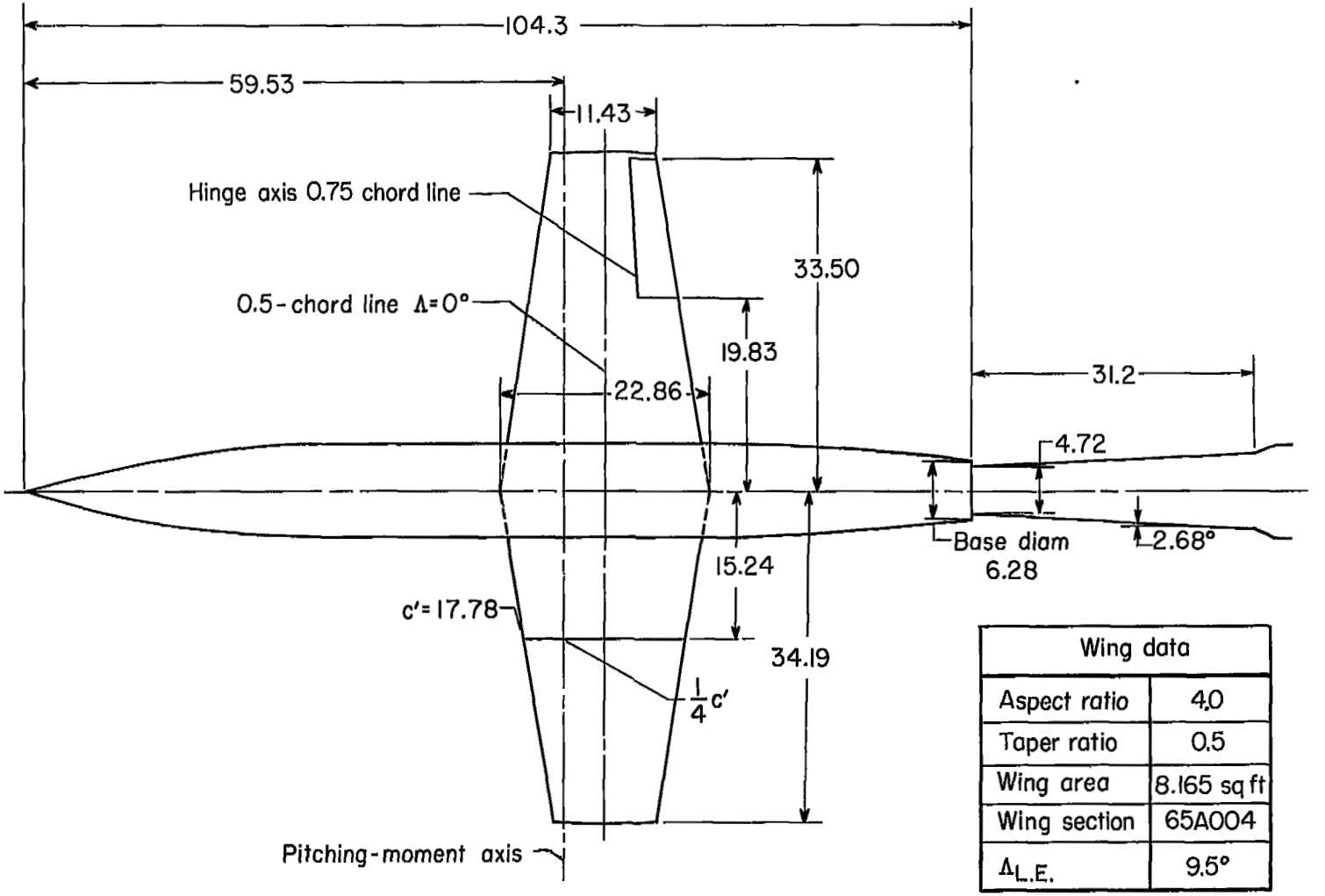

Wing data	
Aspect ratio	4.0
Taper ratio	0.5
Wing area	8.165 sq ft
Wing section	65A004
$\Lambda_{L.E.}$	9.5°

Figure 1.- Geometric details of model. All dimensions are in inches except as noted.

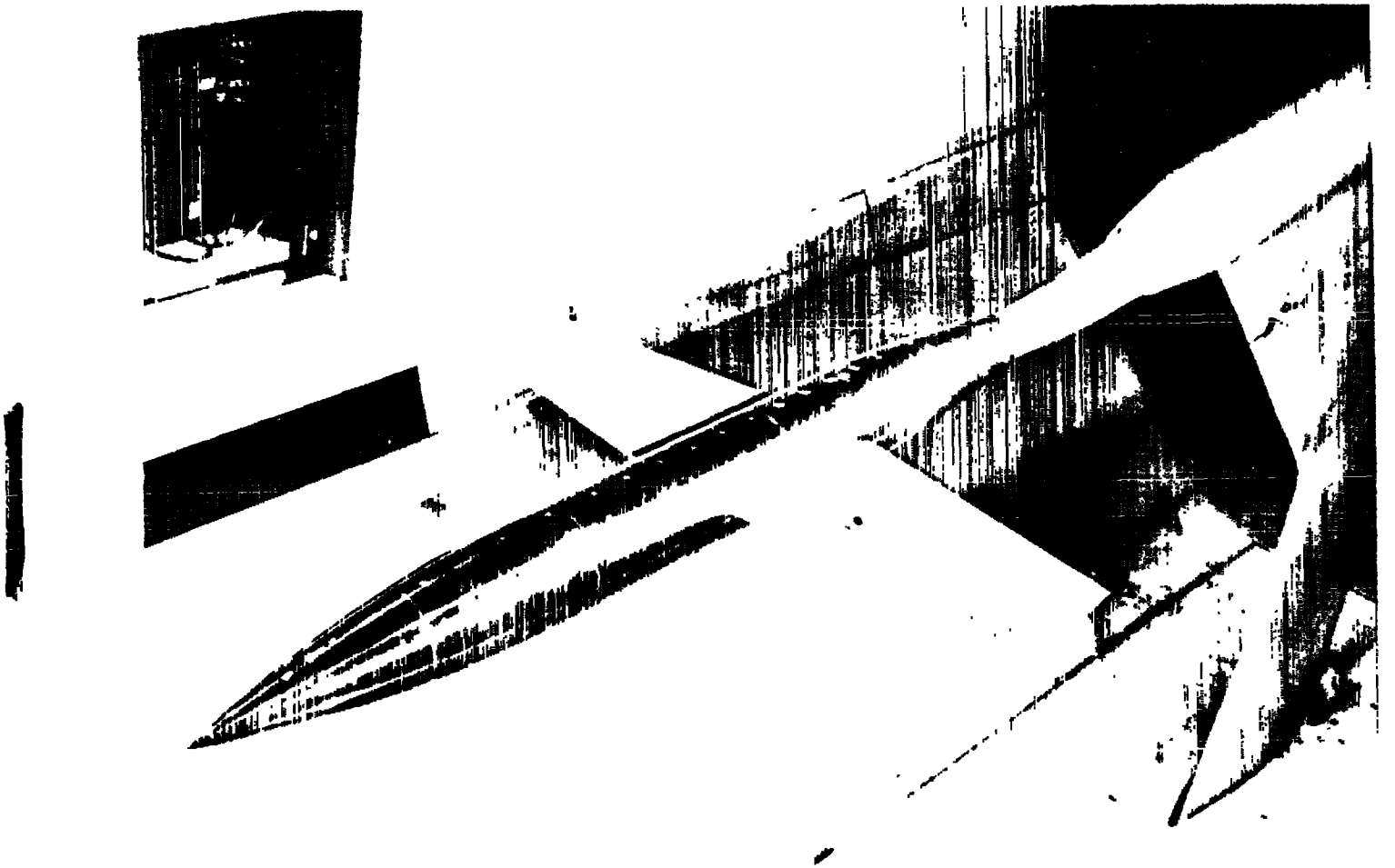

(a) View of complete model. L-80814

Figure 2.- Photographs of model mounted in the tunnel.

L-87867

(b) Top view of aileron and paddle balance.

Figure 2.- Continued.

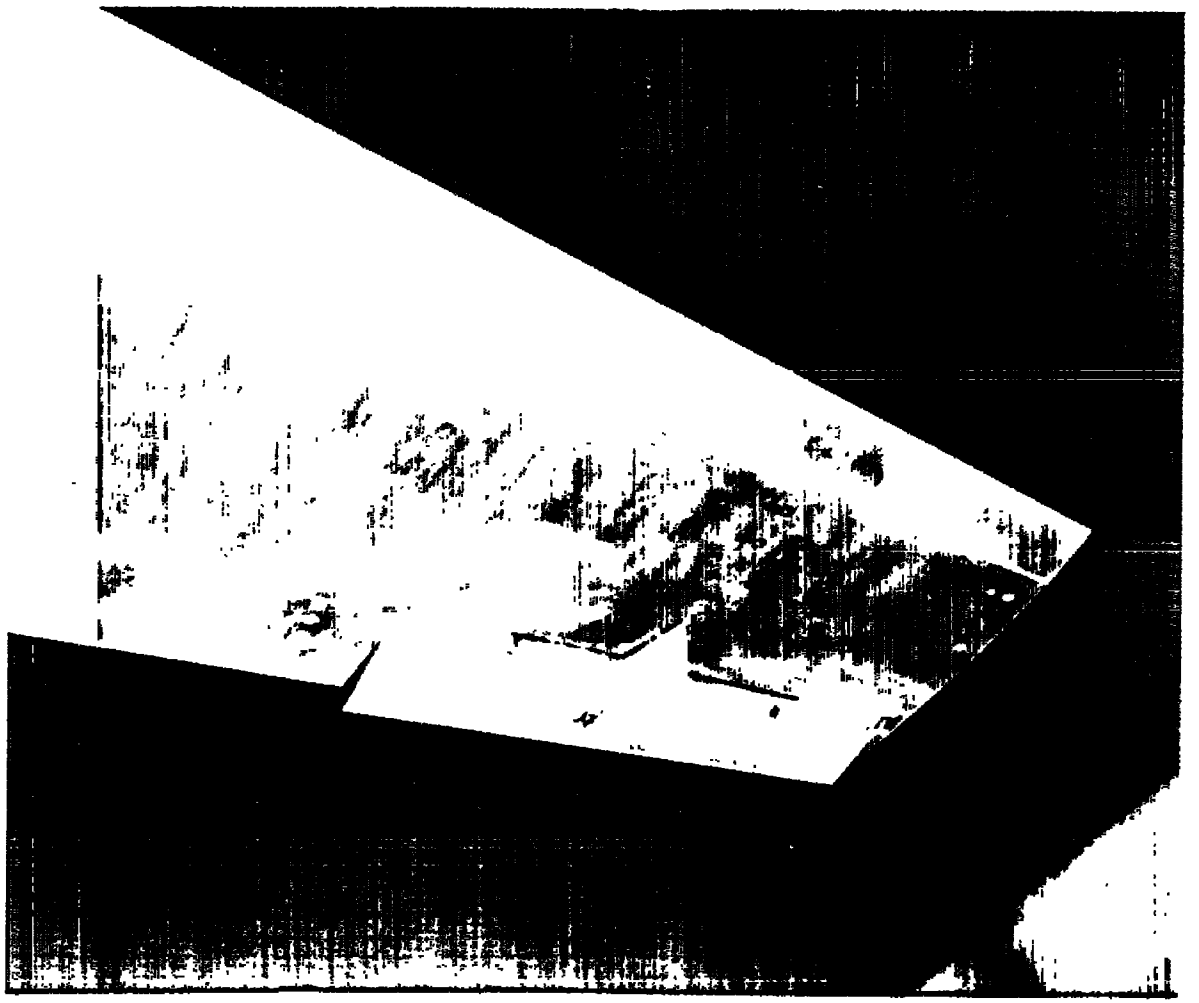

(c) Bottom view of aileron and paddle balance. L-87868

Figure 2.- Concluded.

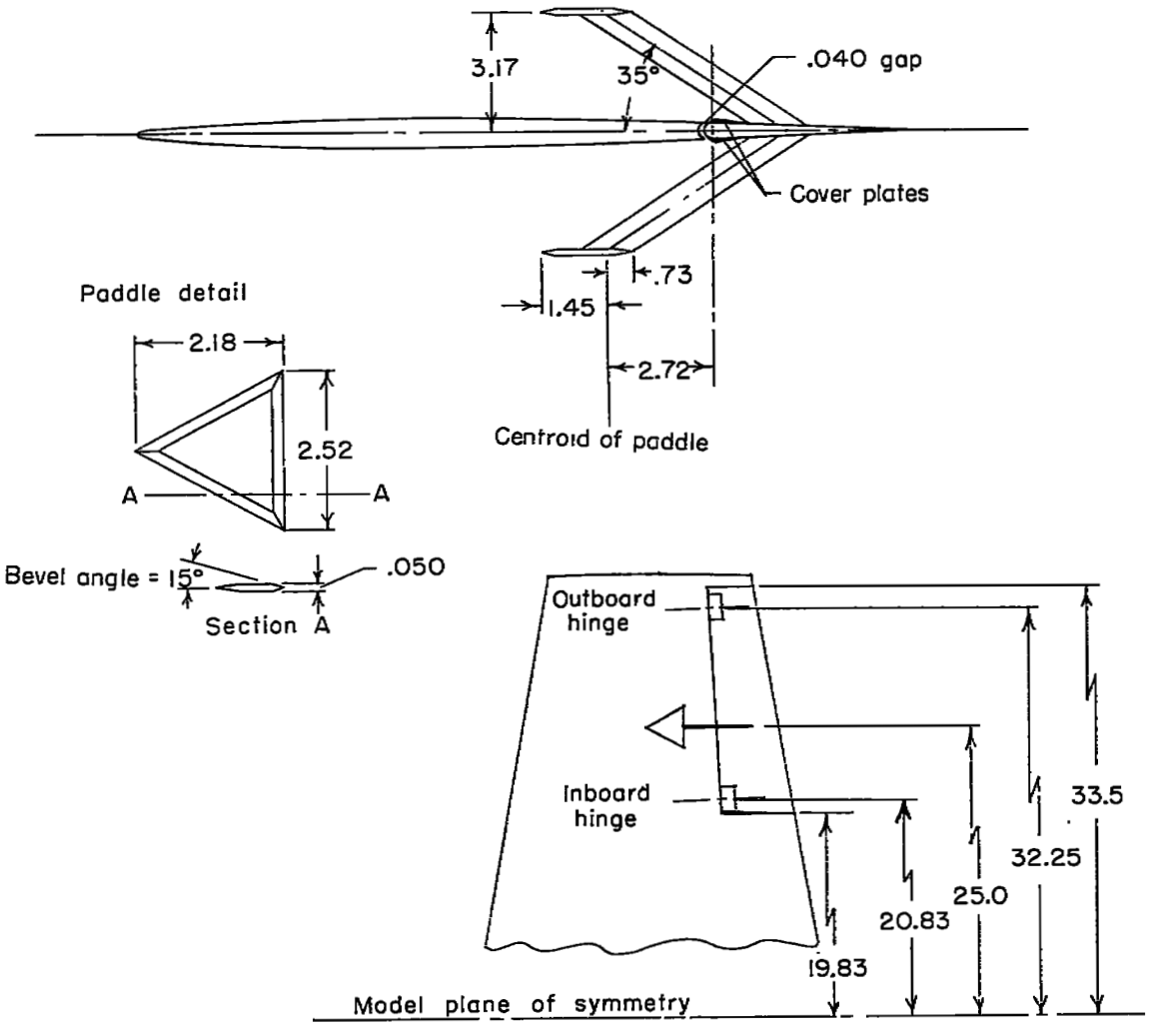

Figure 3.- Aileron and paddle balance details. All dimensions are in inches.

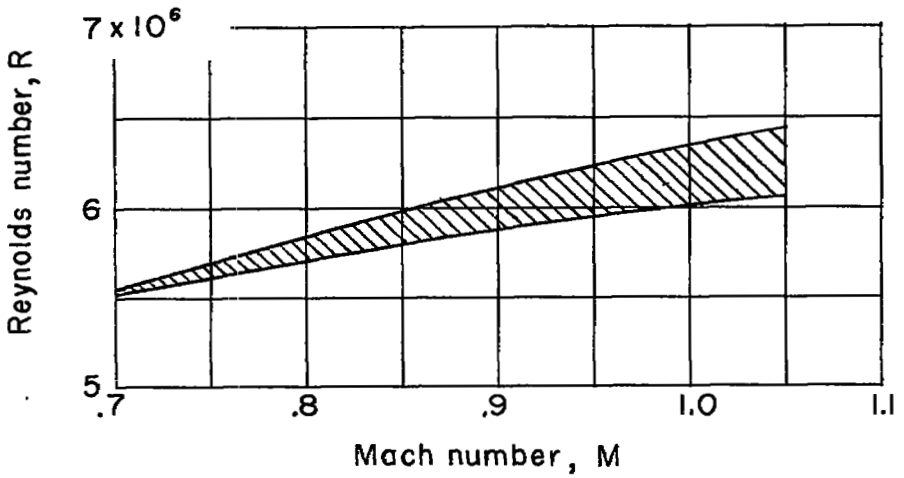

Figure 4.- Variations of Reynolds number with Mach number.

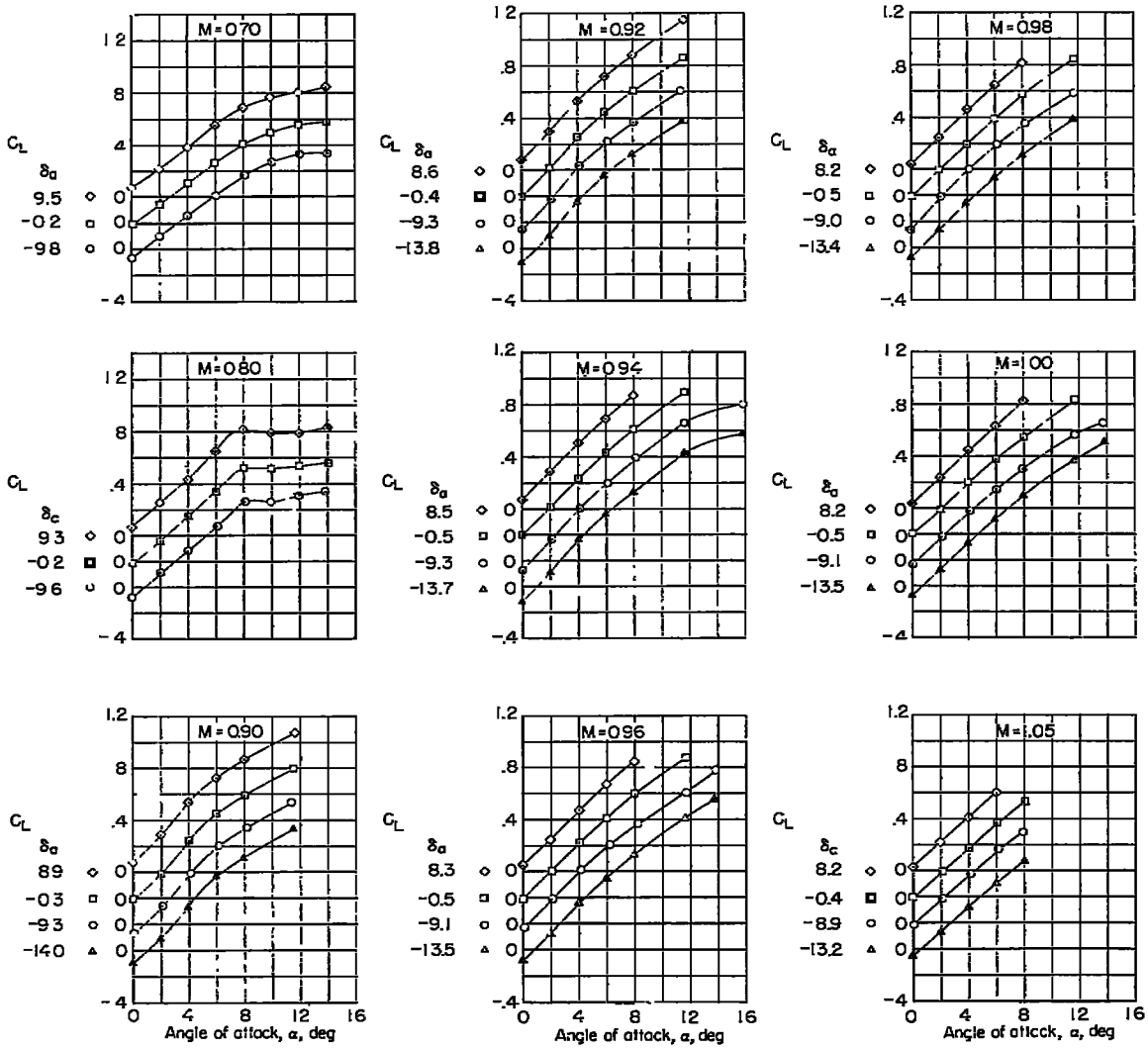

Figure 5.- Model lift characteristics.

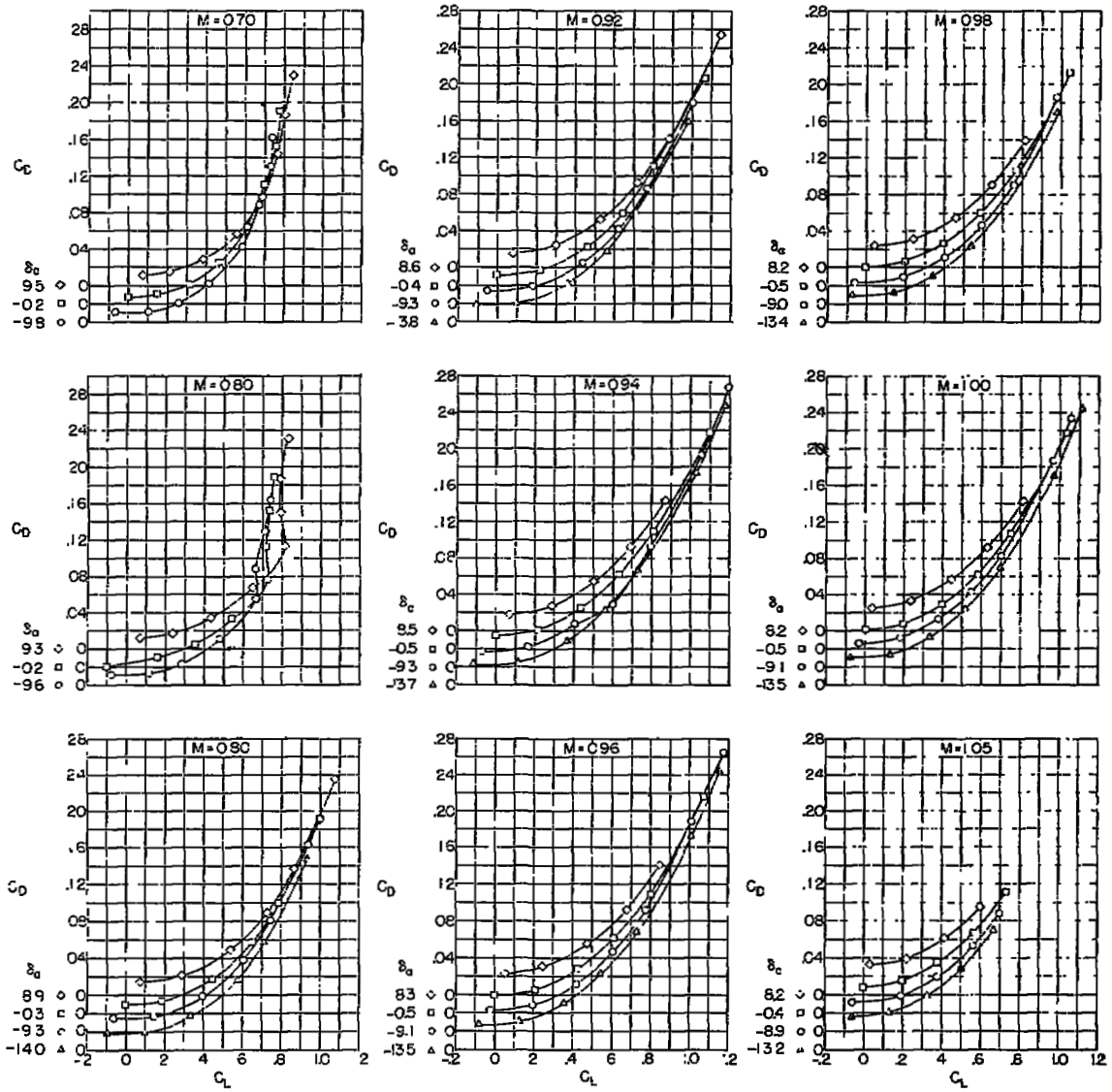

Figure 6.- Model drag characteristics.

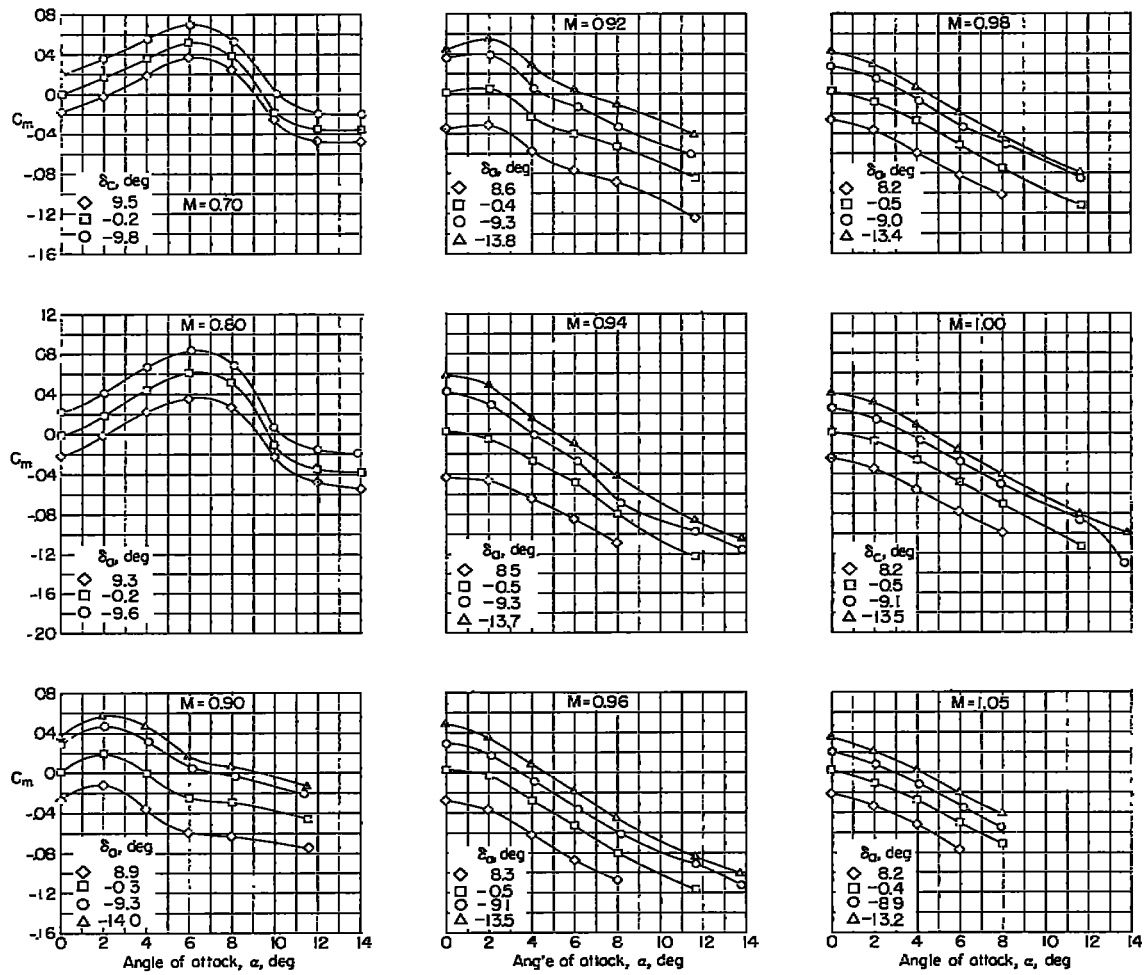

Figure 7.- Model pitching-moment characteristics.

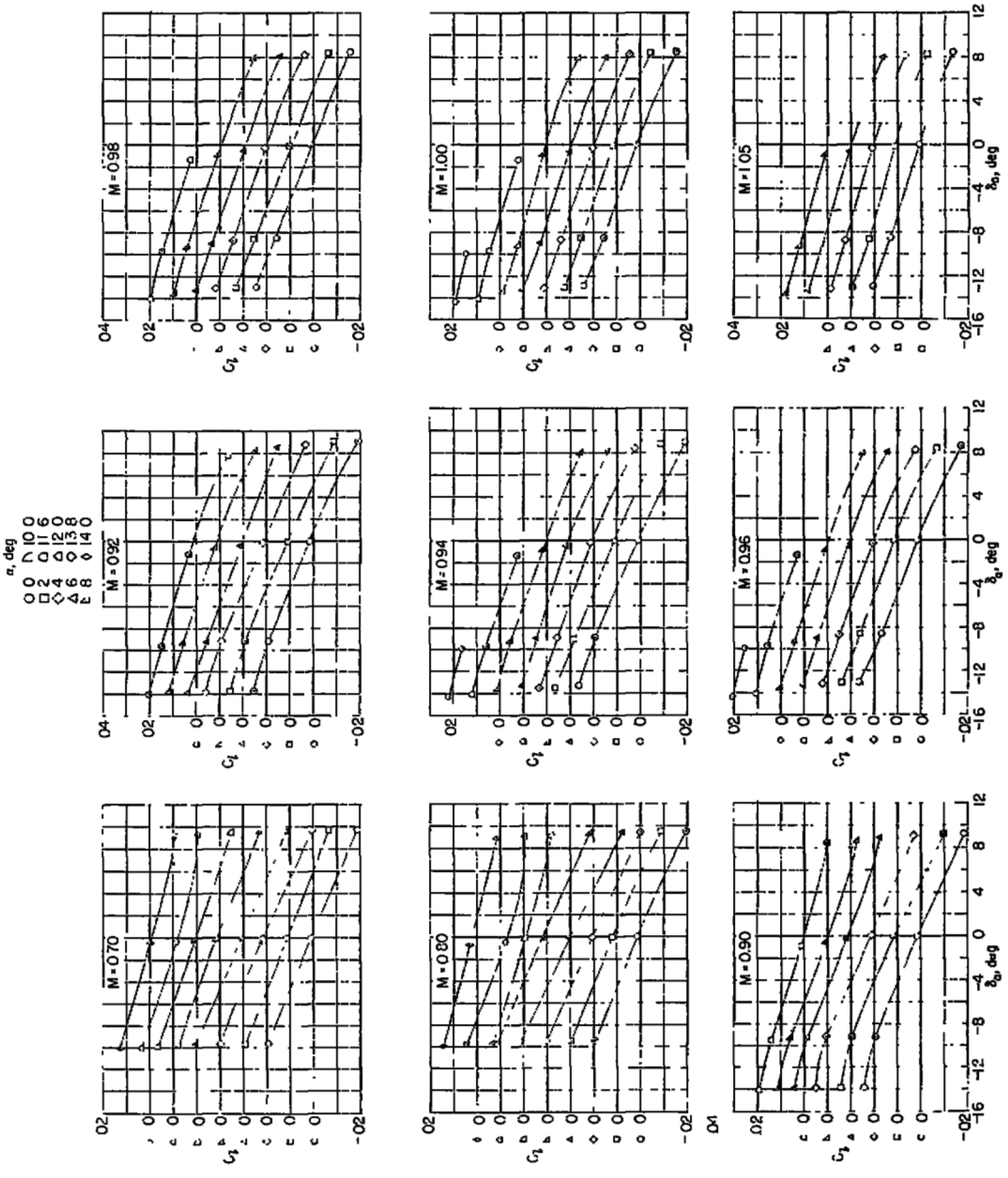

Figure 8.- Model rolling-moment characteristics.

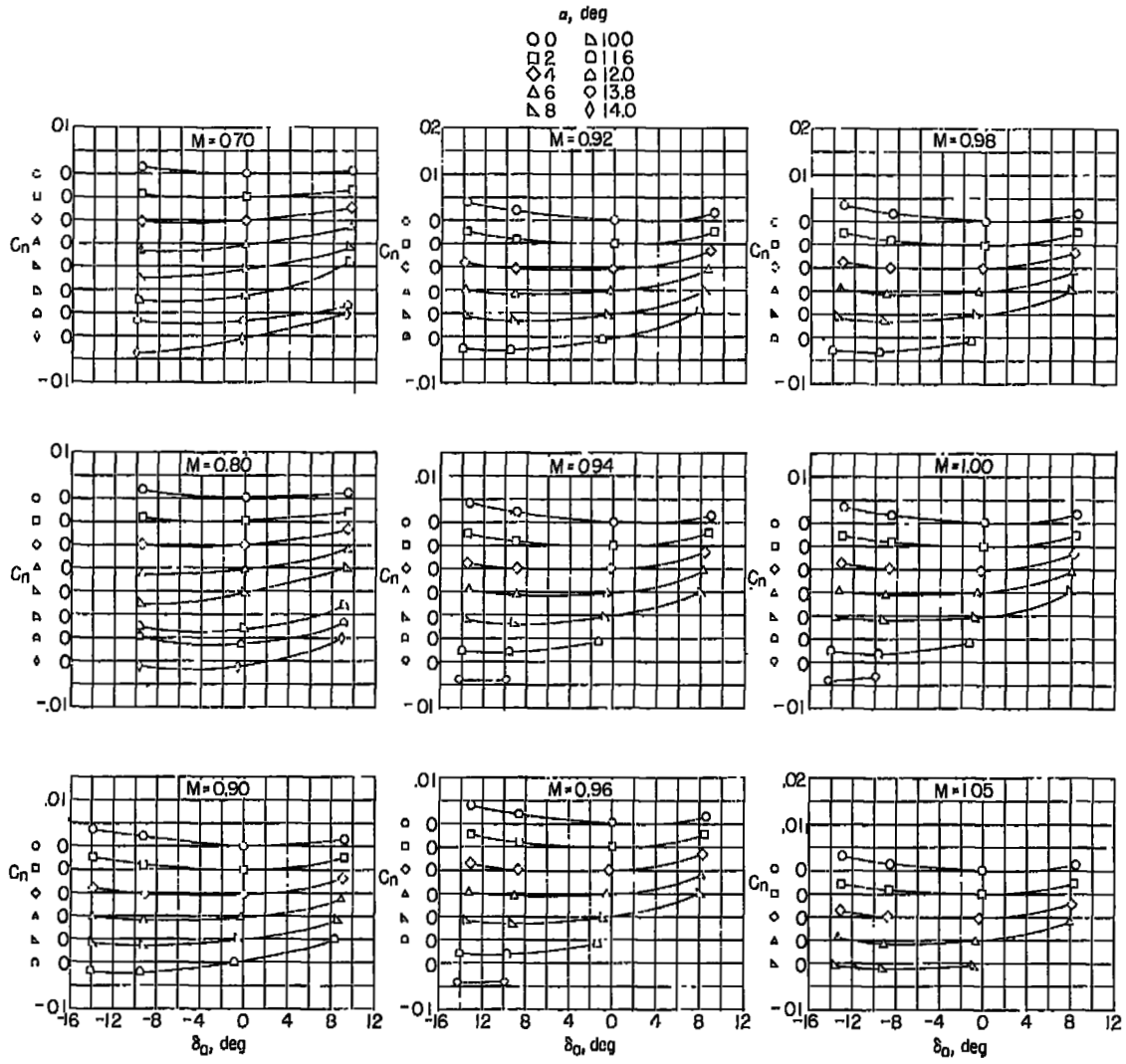

Figure 9.- Model yawing-moment characteristics.

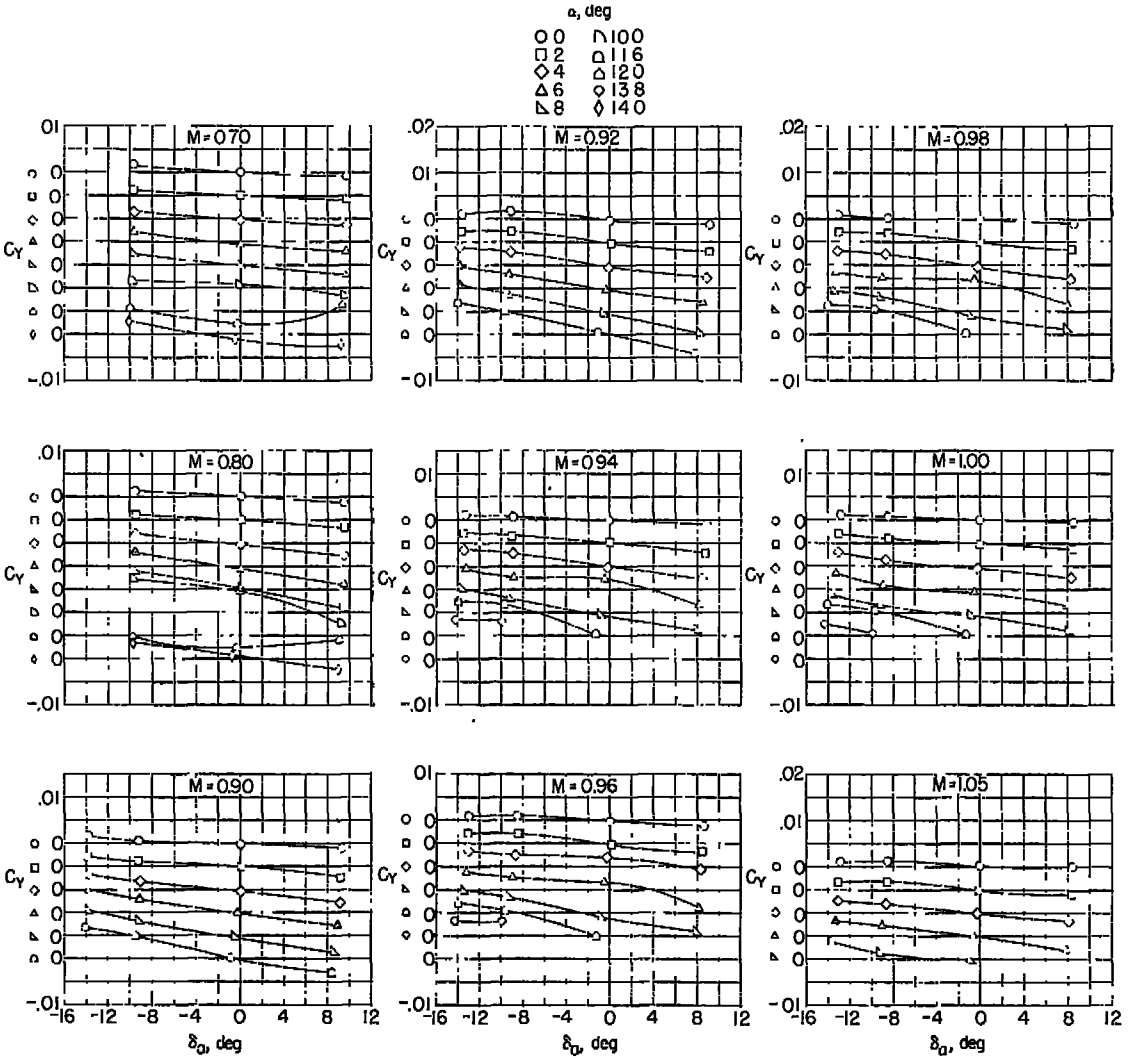

Figure 10.- Model lateral-force characteristics.

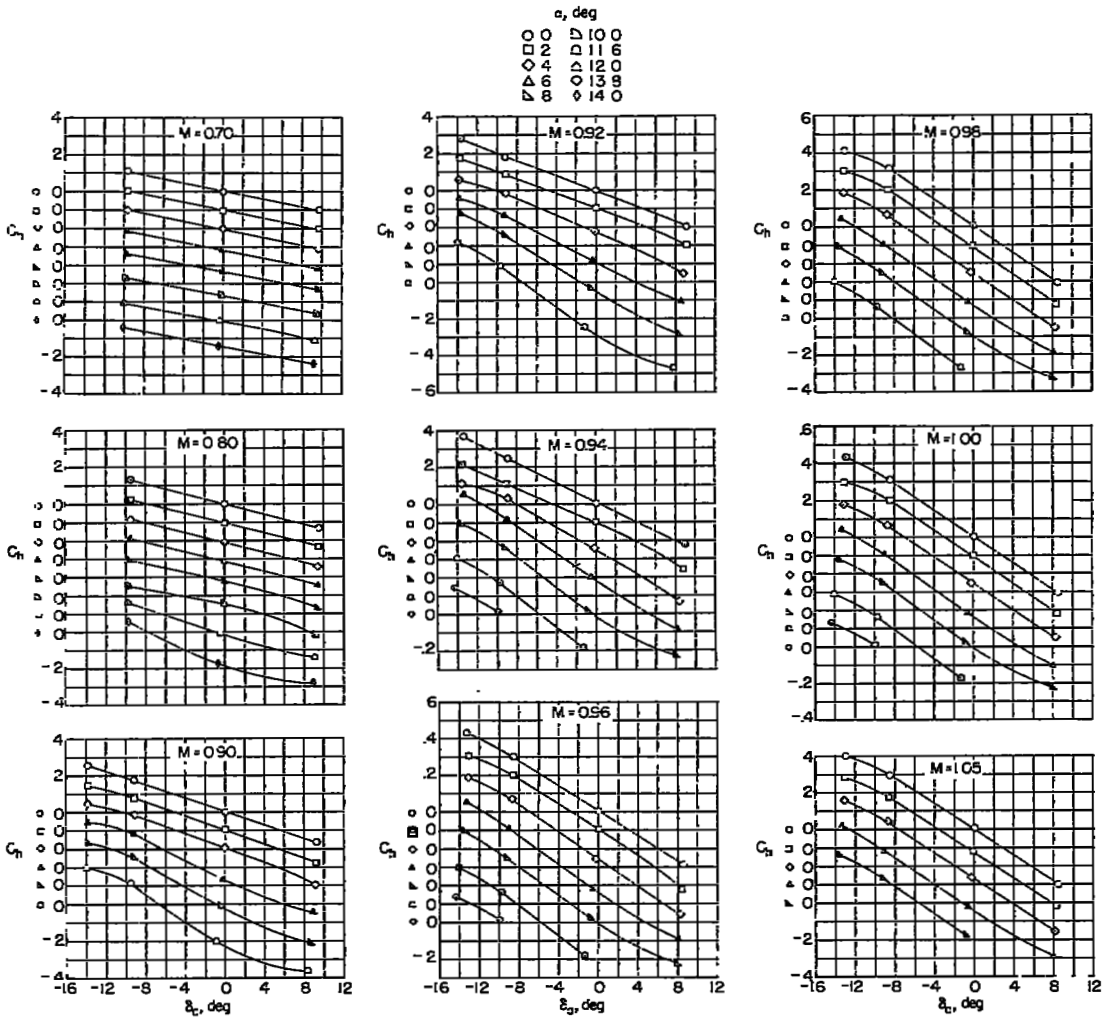

Figure 11.- Aileron hinge-moment characteristics.

[redacted]

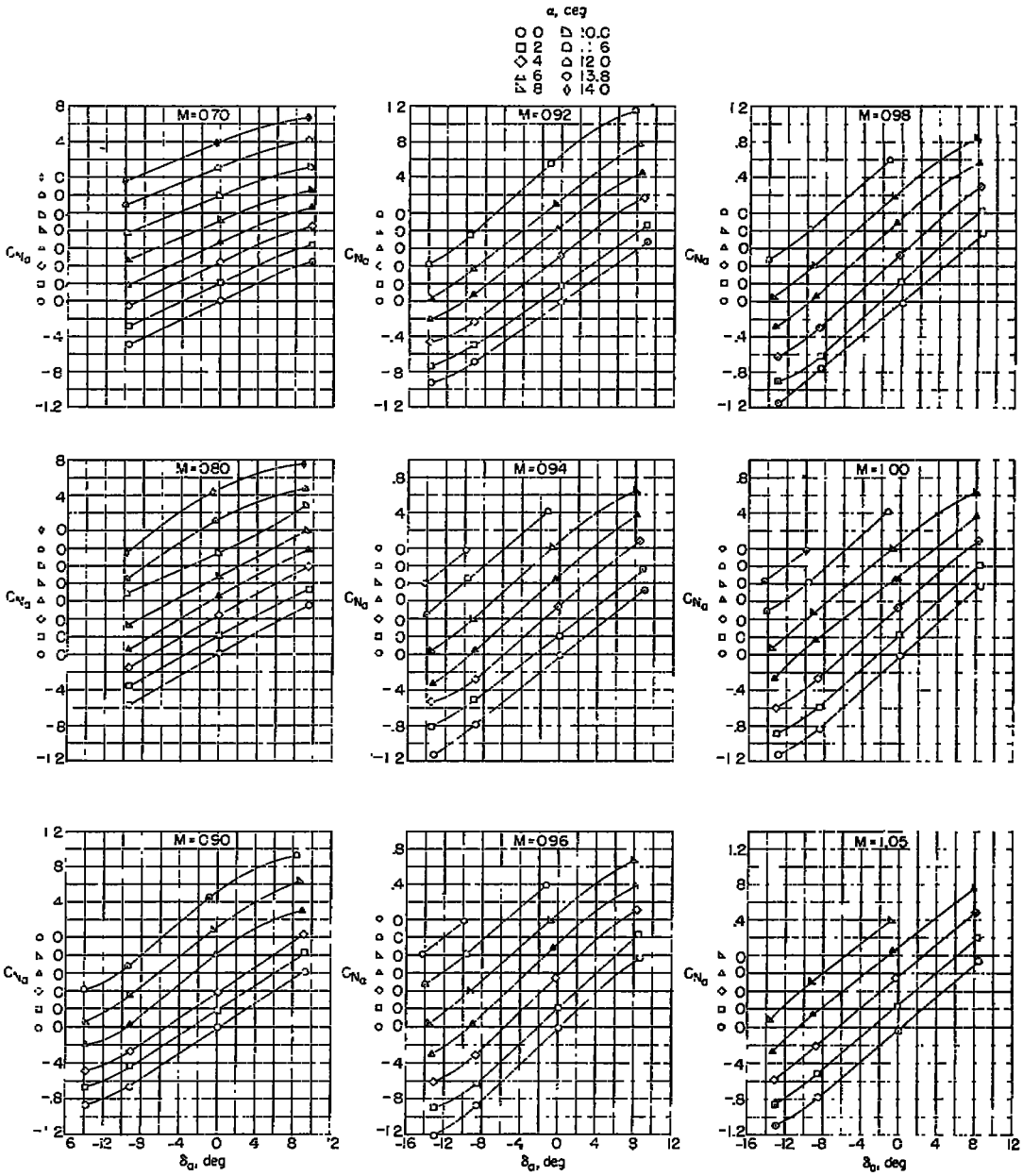

Figure 12.- Aileron normal-force characteristics.

[redacted]

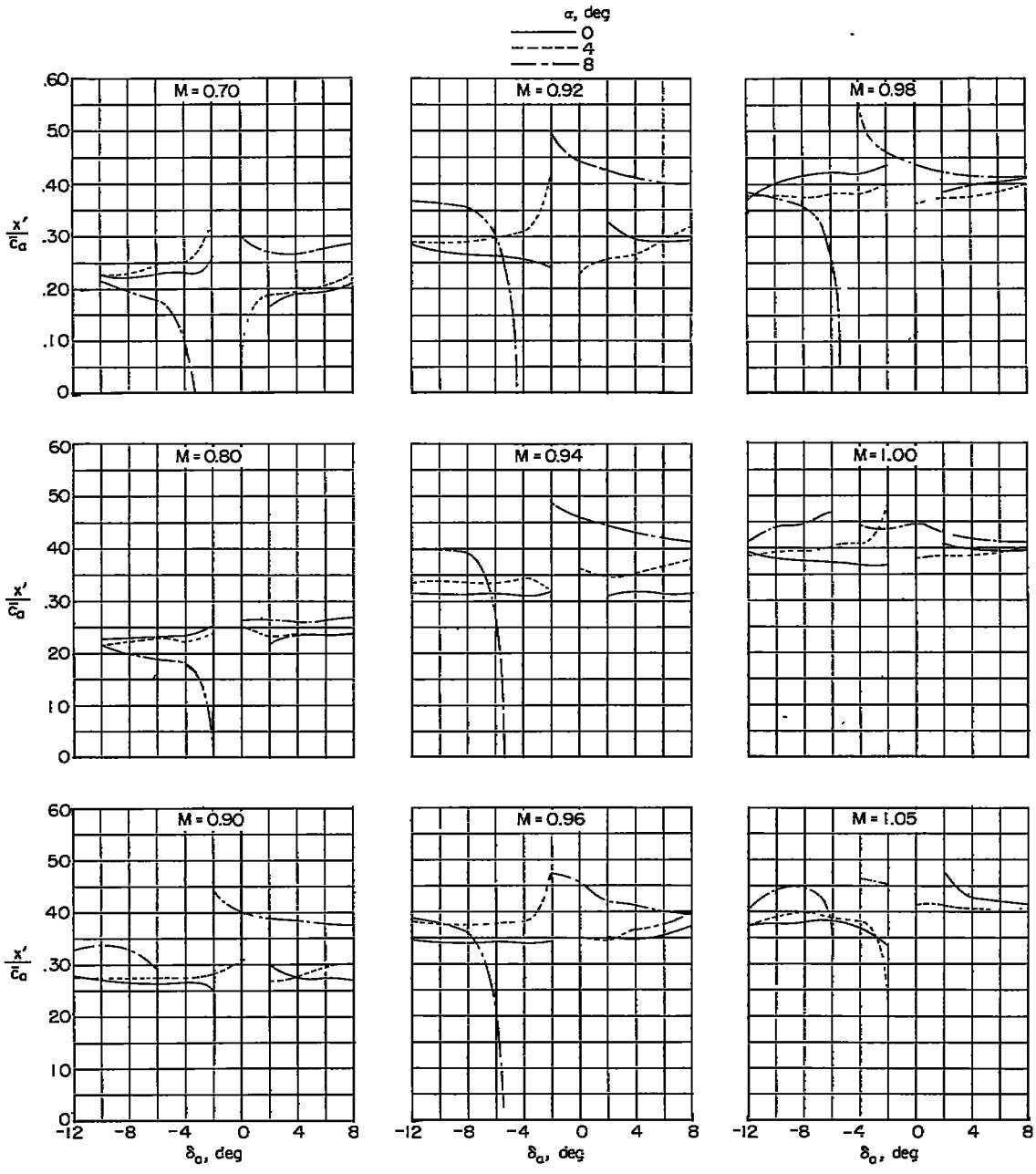

Figure 13.- Aileron chordwise center of pressure.

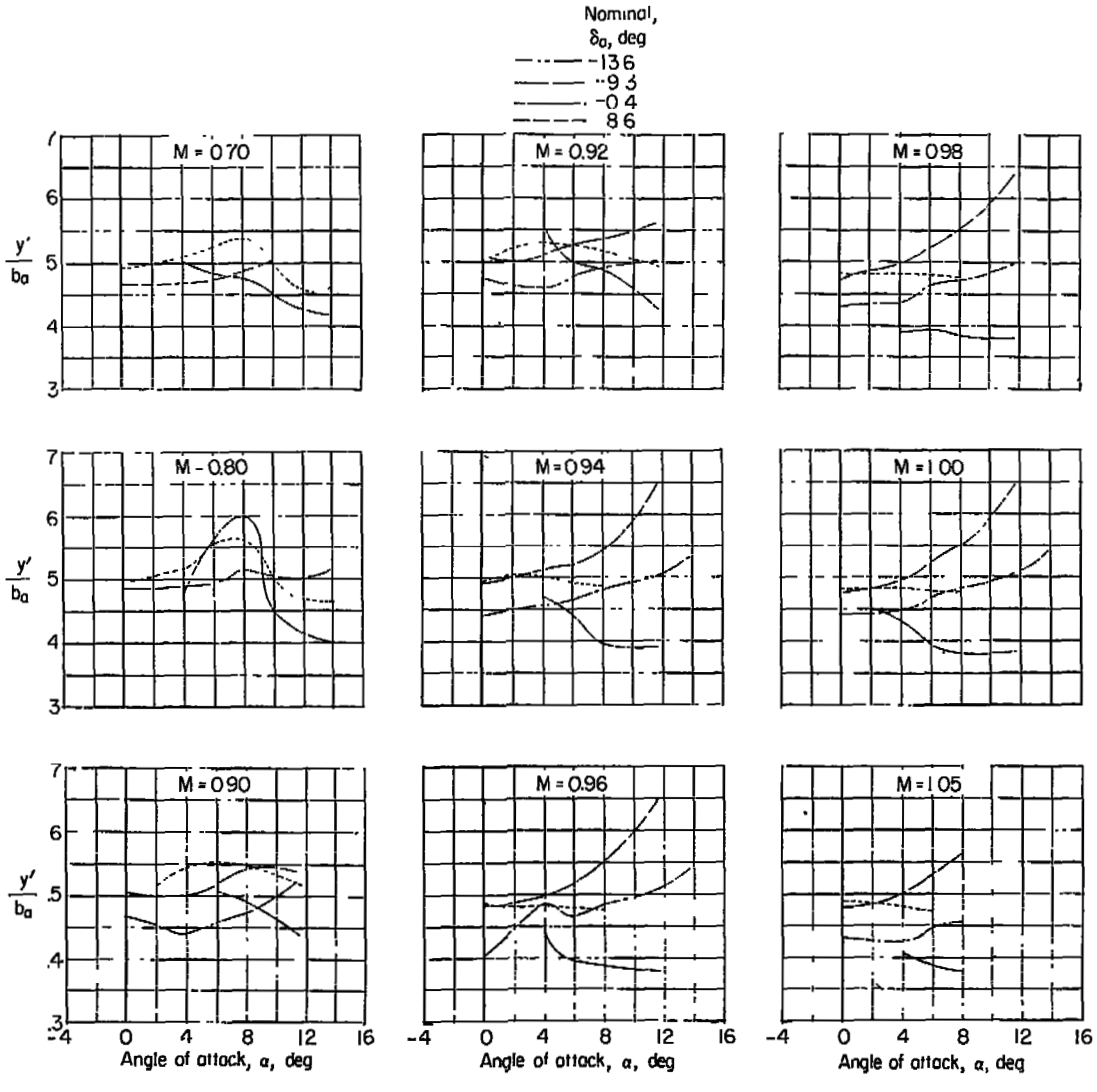

Figure 14.- Aileron lateral center of pressure.

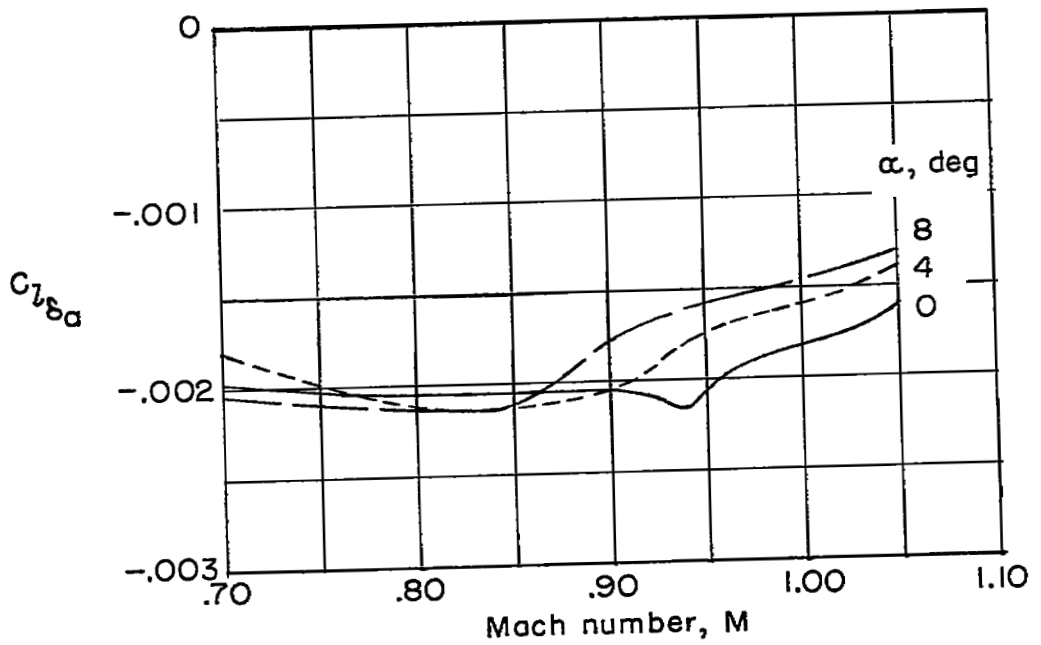

Figure 15.- Effect of Mach number on the effectiveness parameter $C_{l_{\delta_a}}$.

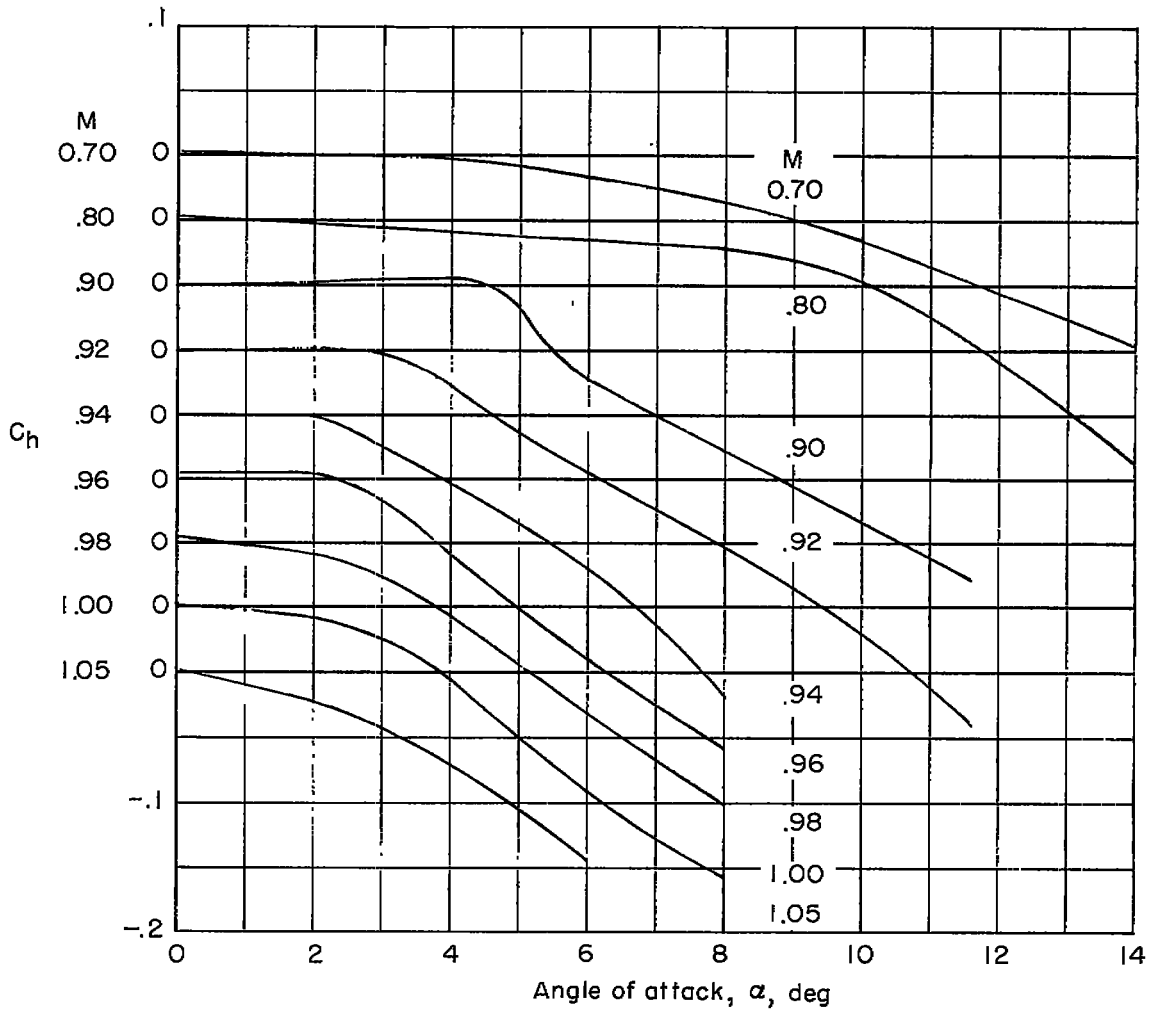

Figure 16.- Variation of hinge-moment coefficient with angle of attack and Mach number. $\delta_a = 0$.

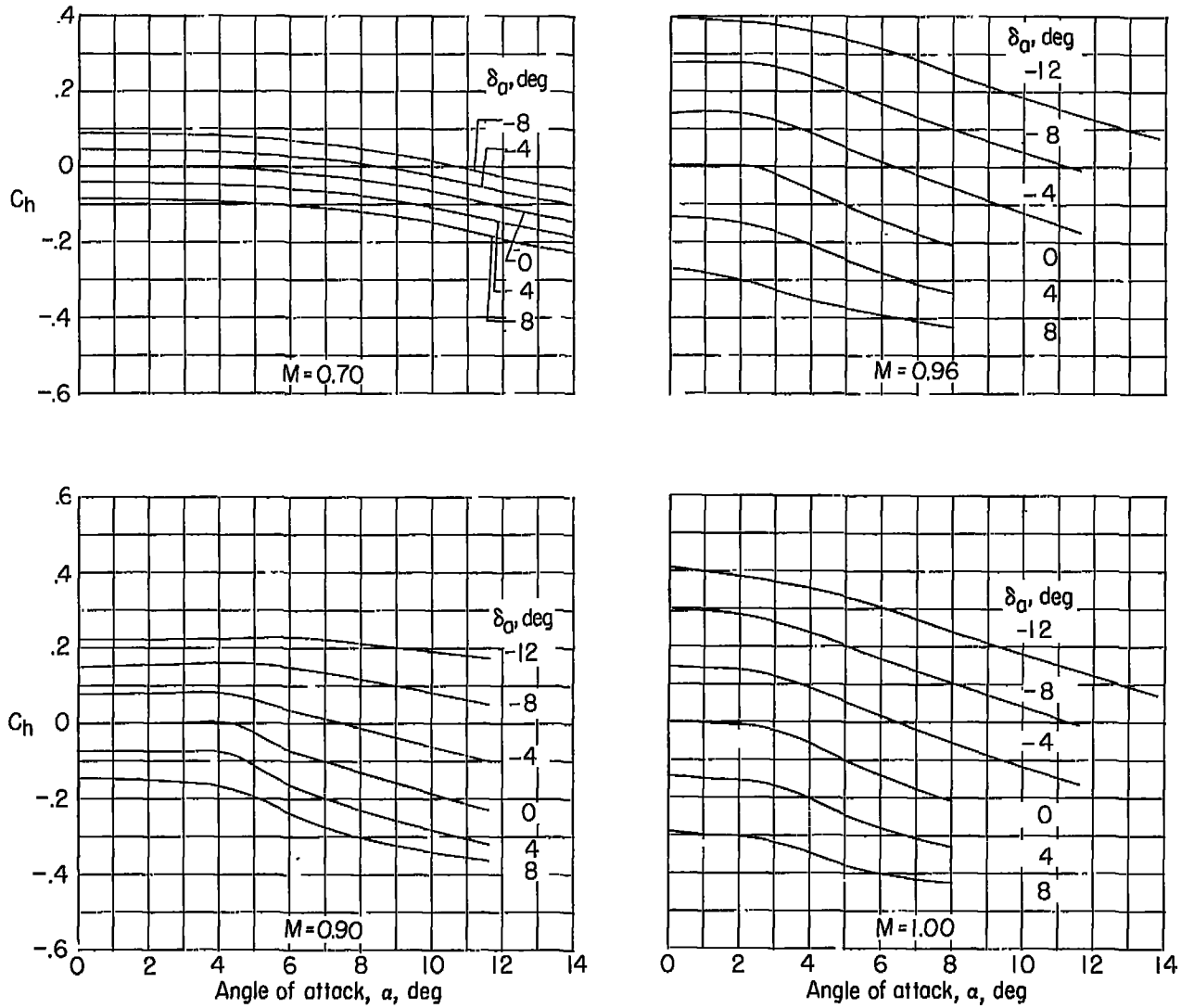

Figure 17.- Variation of hinge-moment coefficient with angle of attack.

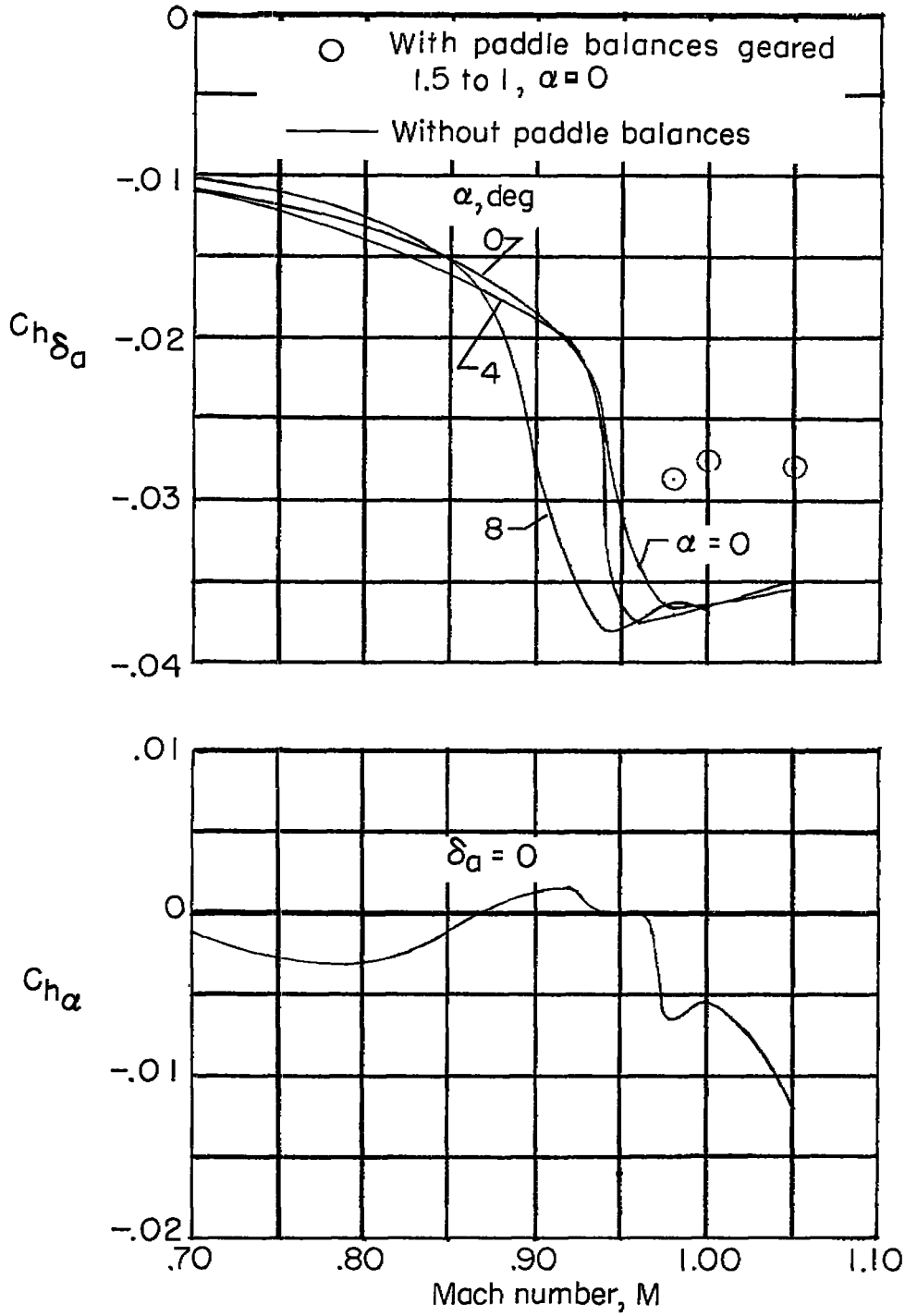

Figure 18.- Effect of Mach number on the parameters $C_{h_{\delta_a}}$ and C_{h_α}.

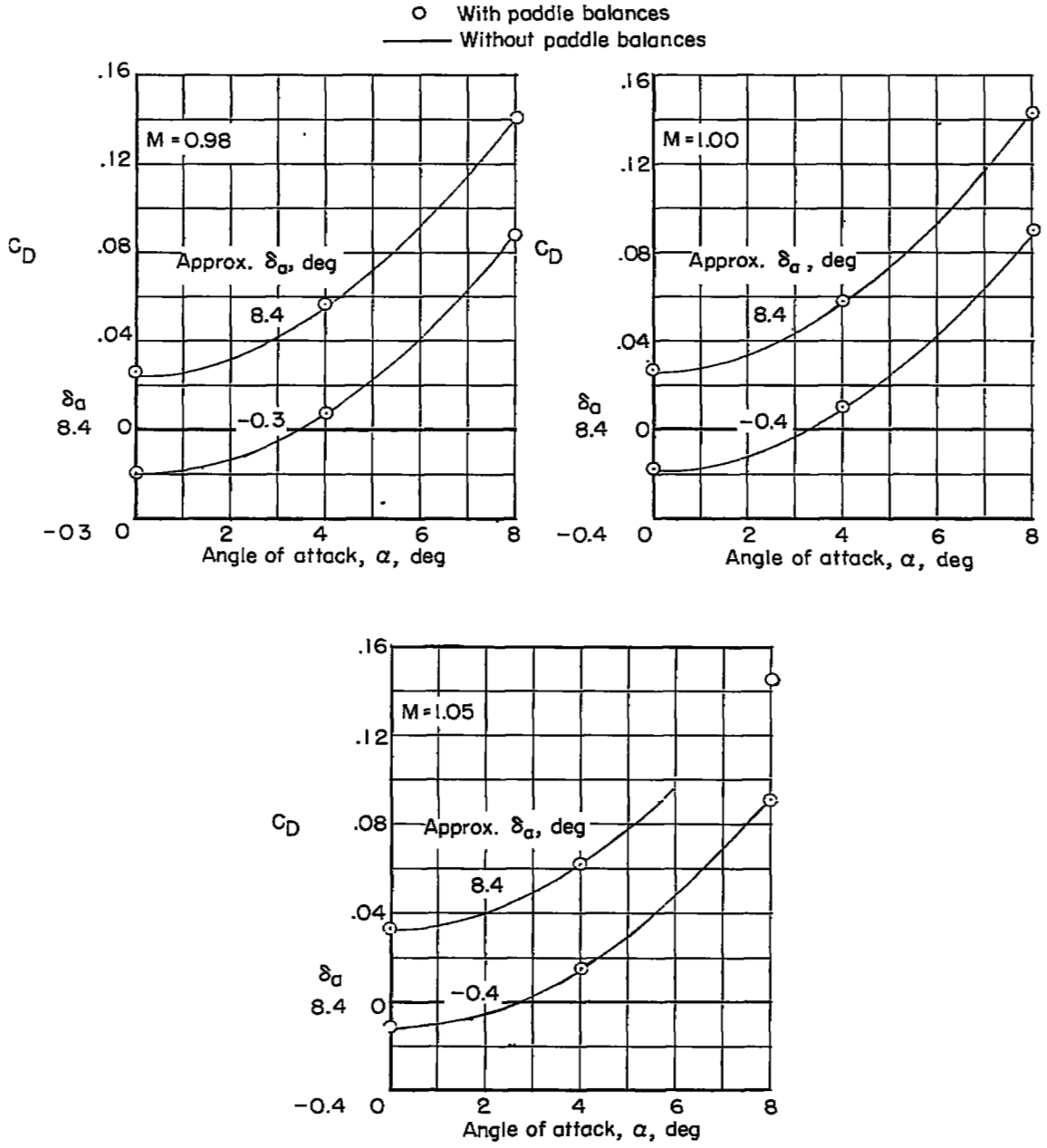

Figure 19.- Effect of paddle balance on model drag coefficient. Nominal paddle-balance gear ratio = 1.5.

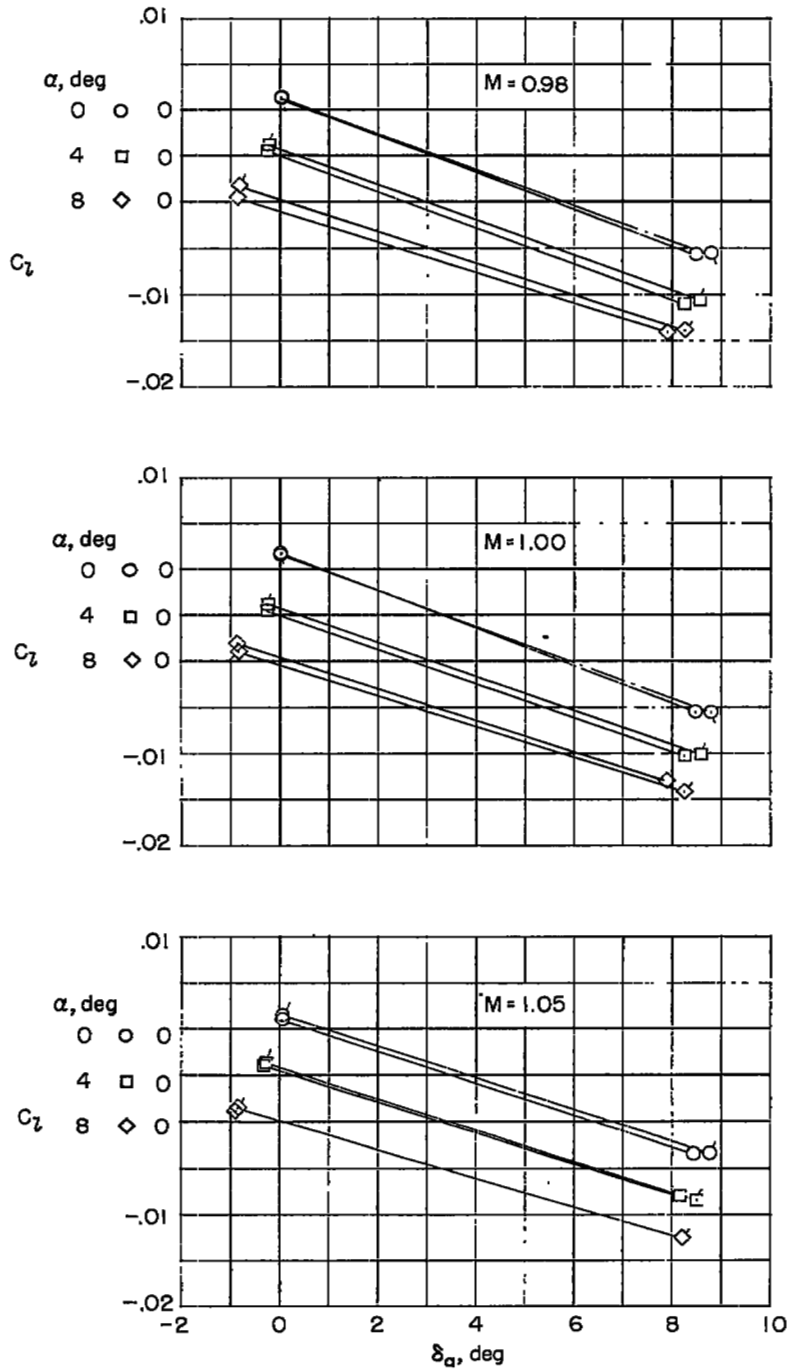

Figure 20.- Effect of paddle balance on rolling-moment coefficient. Flagged symbols denote aileron with paddle balances installed. Nominal paddle-balance gear ratio = 1.5.

CONFIDENTIAL

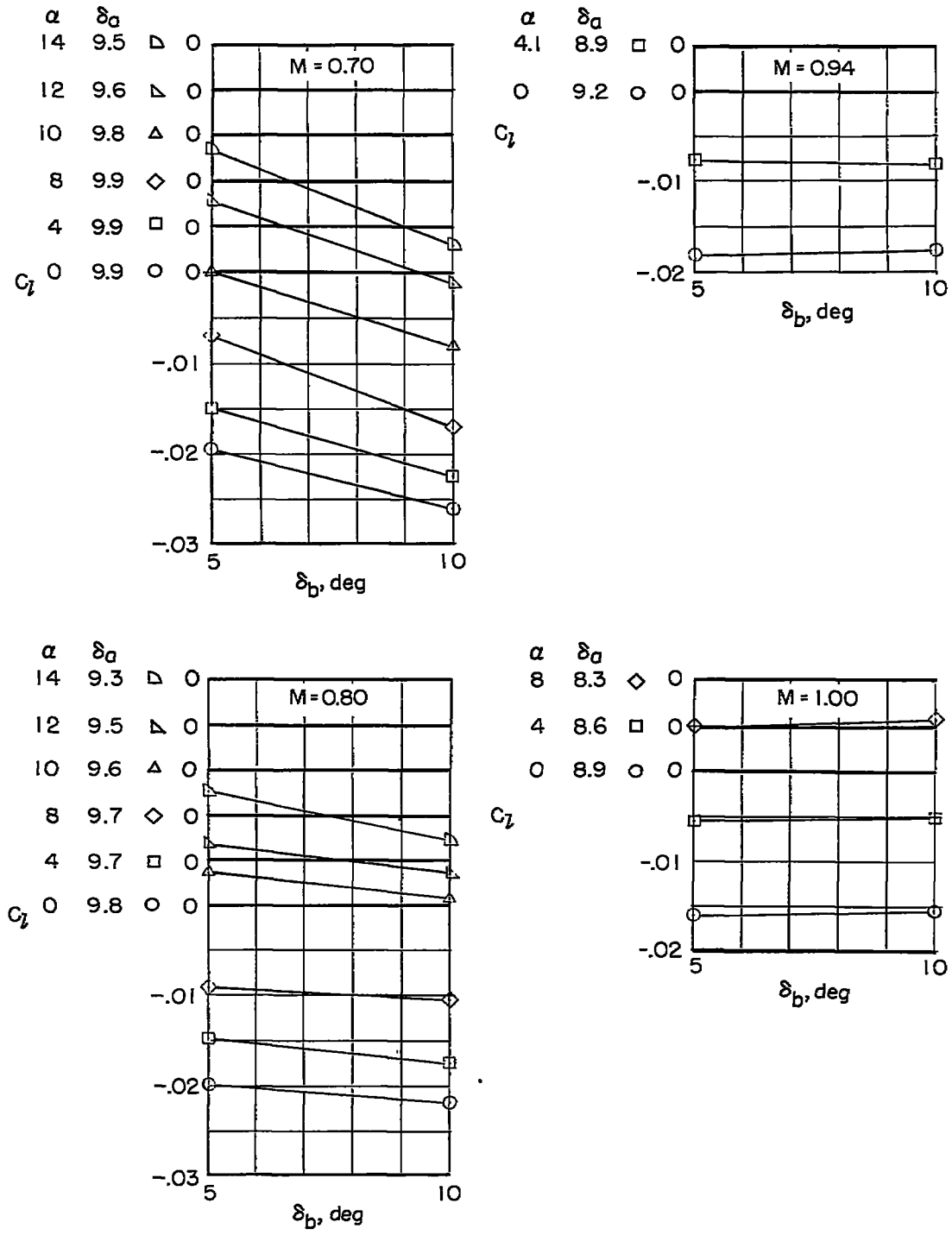

Figure 21.- Variation of rolling-moment coefficient with paddle-balance angle.

[redacted]

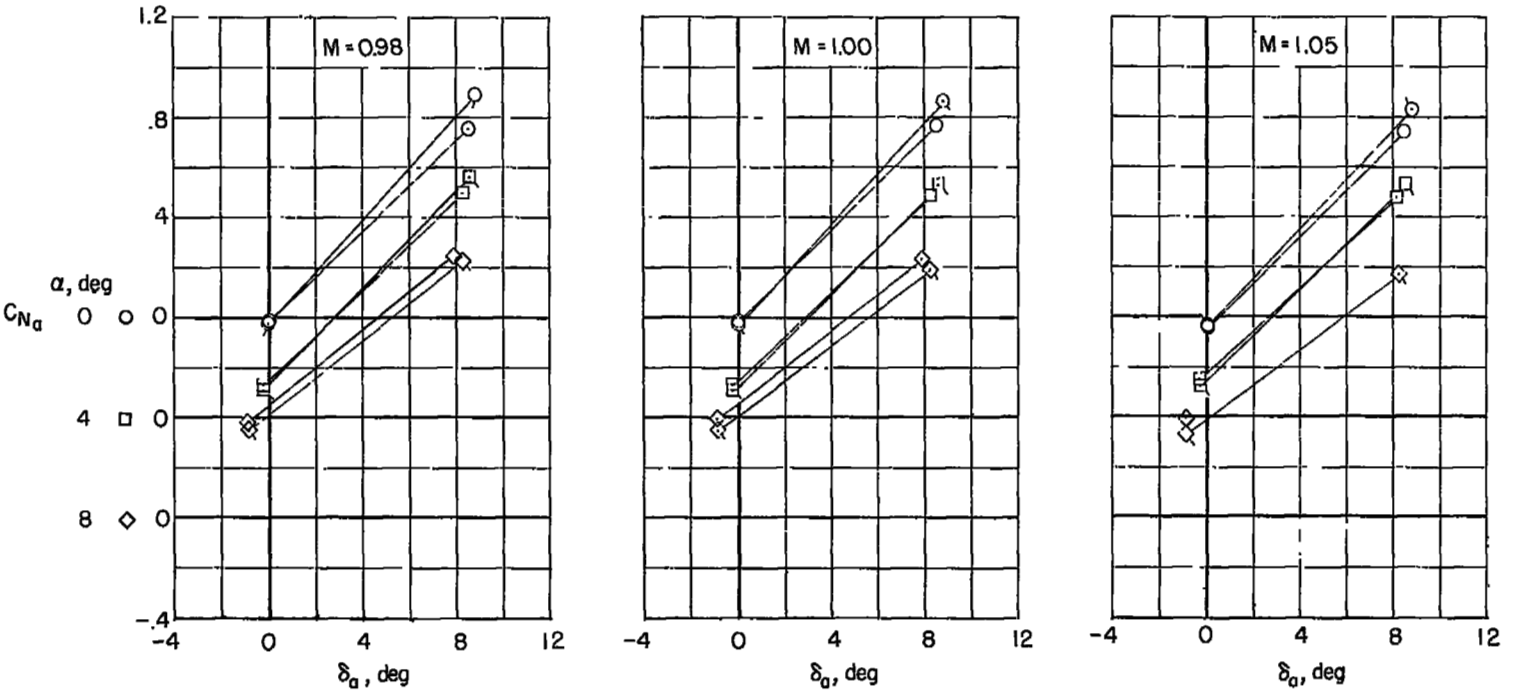

Figure 22.- Effect of paddle balances on aileron normal-force coefficient. Flagged symbols denote aileron with paddle balances installed. Nominal paddle-balance gear ratio = 1.5.

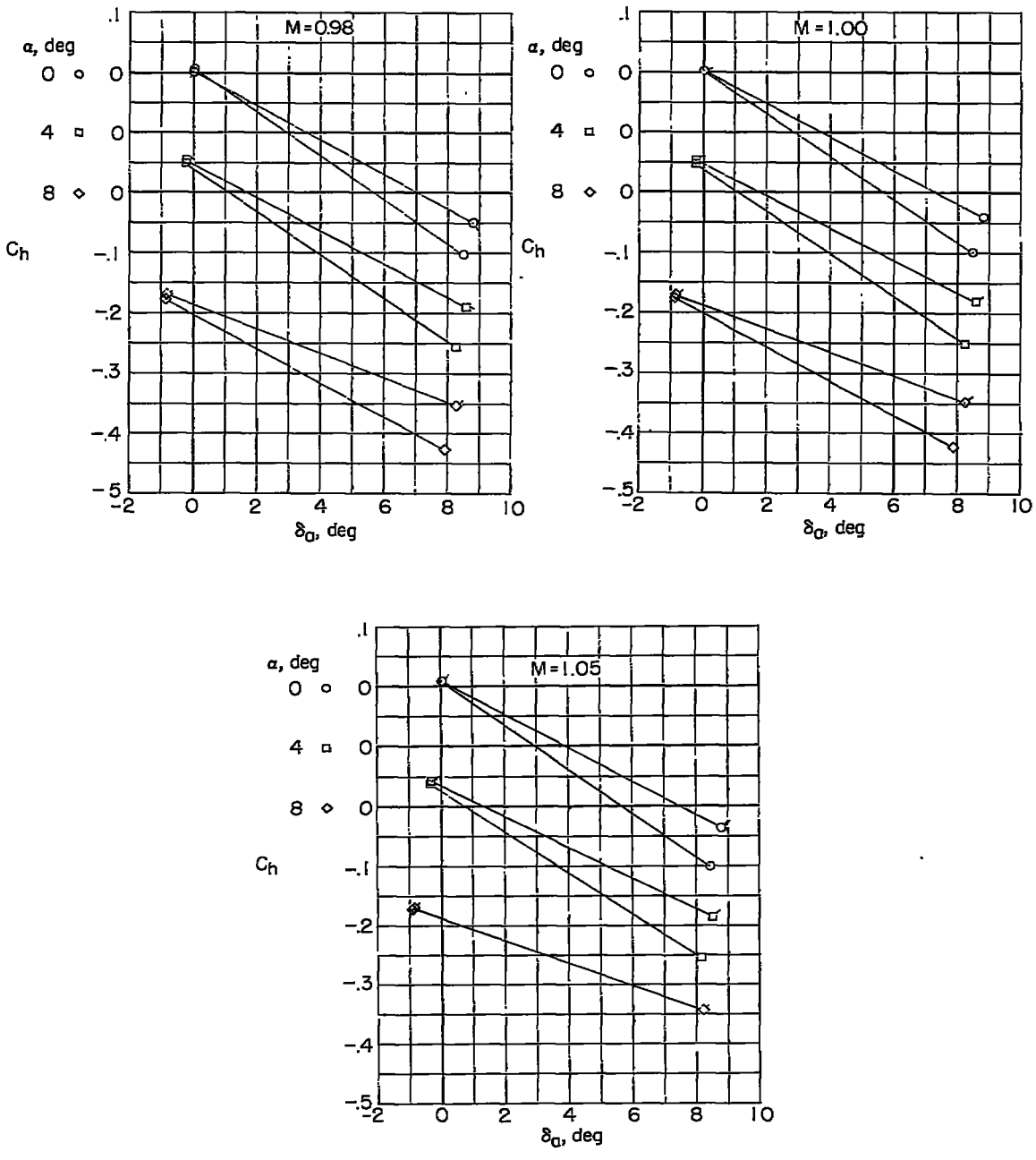

Figure 23.- Effect of paddle balances on aileron hinge-moment coefficient. Flagged symbols denote aileron with paddle balances installed. Nominal paddle-balance gear ratio = 1.5.

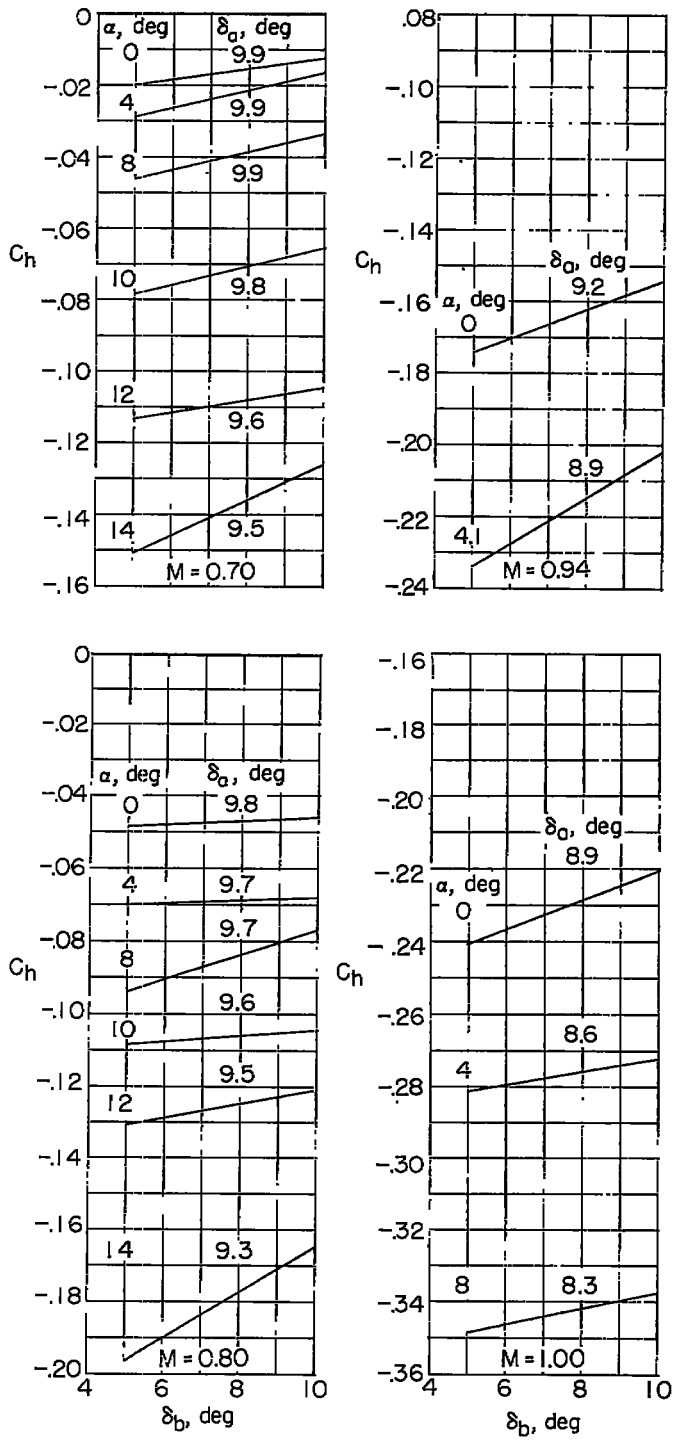

Figure 24.- Variation of hinge-moment coefficient with paddle-balance angle.

[redacted]